Key Points:

- Atmospheric inputs of isotopically light Cd play an important role in setting surface $\delta^{114}Cd$ when surface Cd concentrations are low
- Strong Southern Ocean control on subsurface Cd and $\delta^{114}Cd$ distribution; Antarctic Intermediate Water influences $\delta^{114}Cd$ of North Pacific intermediate waters
- A Cd* minimum at depth in the North Pacific is associated with the PO_4 maximum, a consequence of integrated regeneration

Author Contributions:
Conceptualization: Matthias Sieber, Jessica N. Fitzsimmons, Seth G. John, Tim M. Conway
Formal analysis: Matthias Sieber
Funding acquisition: William M. Landing, Clifton S. Buck, Jessica N. Fitzsimmons, Seth G. John, Tim M. Conway
Investigation: Matthias Sieber, Nathan T. Lanning, Zachary B. Bunnell, Xiaopeng Bian, Shun-Chung Yang, Chris M. Marsay

Biological, Physical, and Atmospheric Controls on the Distribution of Cadmium and Its Isotopes in the Pacific Ocean

Matthias Sieber[1] , Nathan T. Lanning[2], Zachary B. Bunnell[1], Xiaopeng Bian[3] , Shun-Chung Yang[3], Chris M. Marsay[4] , William M. Landing[5] , Clifton S. Buck[4] , Jessica N. Fitzsimmons[2] , Seth G. John[3] , and Tim M. Conway[1]

[1]College of Marine Science, University of South Florida, Tampa, FL, USA, [2]Department of Oceanography, Texas A&M University, College Station, TX, USA, [3]Department of Earth Sciences, University of Southern California, Los Angeles, CA, USA, [4]Skidaway Institute of Oceanography, University of Georgia, Savannah, GA, USA, [5]Department of Earth, Ocean and Atmospheric Science, Florida State University, Tallahassee, FL, USA

Abstract Despite the Pacific being the location of the earliest seawater Cd studies, the processes which control Cd distributions in this region remain incompletely understood, largely due to the sparsity of data. Here, we present dissolved Cd and $\delta^{114}Cd$ data from the US GEOTRACES GP15 meridional transect along 152°W from the Alaskan margin to the equatorial Pacific. Our examination of this region's surface ocean Cd isotope systematics is consistent with previous observations, showing a stark disparity between northern Cd-rich high-nutrient low-chlorophyll waters and Cd-depleted waters of the subtropical and equatorial Pacific. Away from the margin, an open system model ably describes data in Cd-depleted surface waters, but atmospheric inputs of isotopically light Cd likely play an important role in setting surface Cd isotope ratios ($\delta^{114}Cd$) at the lowest Cd concentrations. Below the surface, Southern Ocean processes and water mass mixing are the dominant control on Pacific Cd and $\delta^{114}Cd$ distributions. Cd-depleted Antarctic Intermediate Water has a far-reaching effect on North Pacific intermediate waters as far as 47°N, contrasting with northern-sourced Cd signatures in North Pacific Intermediate Water. Finally, we show that the previously identified negative Cd* signal at depth in the North Pacific is associated with the PO_4 maximum and is thus a consequence of an integrated regeneration signal of Cd and PO_4 at a slightly lower Cd:P ratio than the deep ocean ratio (0.35 mmol mol^{-1}), rather than being related to in situ removal processes in low-oxygen waters.

1. Introduction

Seawater concentrations of the trace element cadmium (Cd) are closely correlated with those of the macronutrient phosphate (PO_4, Boyle et al., 1976; de Baar et al., 1994). This nutrient-type behavior is a consequence of uptake of Cd by phytoplankton in surface waters and remineralization at depth, resulting in large-scale Cd distributions similar to major nutrients like PO_4. While the exact physiological role of Cd remains unknown, there is clear evidence from culturing studies that Cd can act as a micronutrient under zinc-limiting conditions (Price & Morel, 1990), in spite of its known toxicity (Brand et al., 1986). Furthermore, Cd uptake has been linked to availability of other micronutrients like iron (Fe) and zinc (Zn) suggesting common uptake pathways (Cullen, 2006; Sunda & Huntsman, 2000) or accidental uptake (Horner et al., 2013). There is a large range in the stoichiometry of phytoplankton Cd uptake, with uptake rates increasing with ambient Cd concentrations and under Zn- or Fe-limiting conditions (Cullen et al., 2003; Sunda & Huntsman, 2000). Consequently, elevated phytoplankton uptake of Cd relative to PO_4 in the surface Southern Ocean, coupled with water mass formation and mixing, are the main drivers of the global marine Cd distribution and its relationship to PO_4 (Middag et al., 2018). Despite large variability in the cadmium:phosphorous (Cd:P) uptake ratio, and consequently the Cd:P export ratio (e.g., Black et al., 2019; Bourne et al., 2018; Sunda & Huntsman, 2000), remineralization is only thought to cause smaller-scale variations in the Cd-PO_4 relationship, mostly restricted to the upper ocean (Middag et al., 2018; Wu & Roshan, 2015).

The tracer Cd*, while implying nothing about the source of deviations in Cd:P, is commonly used to identify (and quantify) deviations of Cd concentration from its established correlation with PO_4 (e.g., Baars et al., 2014; de Souza et al., 2022; Janssen et al., 2014). For the purposes of our study, we define Cd* using the following equation, with the deep Pacific Ocean Cd:PO_4 ratio as a reference point, used by the North Pacific study of Janssen et al. (2014) for ease of comparison to existing studies in the region:

Writing – original draft: Matthias Sieber, Tim M. Conway
Writing – review & editing: Matthias Sieber, Nathan T. Lanning, Zachary B. Bunnell, Xiaopeng Bian, Chris M. Marsay, William M. Landing, Clifton S. Buck, Jessica N. Fitzsimmons, Seth G. John, Tim M. Conway

$$Cd^* = Cd - PO_4 \times 0.35\ \mathrm{mmol\ mol^{-1}}$$

Globally, and most notably, data from the upper part of oceanic oxygen minimum zones (OMZs) exhibit negative Cd* values, indicating an apparent dissolved Cd-deficit relative to dissolved PO_4 (Conway & John, 2015a; Guinoiseau et al., 2019; Janssen et al., 2014). This Cd* signal was initially suggested to reflect a loss of dissolved Cd via precipitation of cadmium sulfide (CdS) associated with anoxic-microenvironments within sinking particles (Janssen et al., 2014); however, this interpretation has remained controversial (e.g., John et al., 2018; Xie et al., 2018). Regeneration effects, heterotrophic uptake, or water mass mixing are other possible sources of Cd* deviations in OMZ waters (Bourne et al., 2018; de Souza et al., 2022; Ohnemus et al., 2019; Roshan & DeVries, 2021). Consequently, the cause of the apparent Cd-deficit observed at intermediate OMZ depths in the North Pacific remains unclear but is likely driven by the interaction between physical circulation and the variable stoichiometry of biological Cd uptake and regeneration at high and low latitudes (Bourne et al., 2018; de Souza et al., 2022; Quay et al., 2015; Roshan & Wu, 2015).

In the last decade, stimulated largely by the international GEOTRACES program, studies of the distribution of the isotopic composition of dissolved Cd (δ^{114}Cd) have proven to be a useful tool to gain insights into the processes controlling the spatial distribution of Cd and its relationship to macronutrients (e.g., Abouchami et al., 2014; Conway & John, 2015a; Sieber, Conway, de Souza, Obata, et al., 2019). Culturing experiments have shown that phytoplankton preferentially take up light Cd (John & Conway, 2014; Lacan et al., 2006), which is consistent with elevated δ^{114}Cd observed in surface waters (Abouchami et al., 2011; Janssen et al., 2017; Sieber, Conway, de Souza, Hassler, et al., 2019). Isotope systematics associated with Cd uptake have been modeled using closed-system Rayleigh fractionation for waters in high-nutrient low-chlorophyll (HNLC) regions with elevated Cd concentrations (fractionation factor α ranging from 0.9993 to 0.9999, where $\alpha = R_{\mathrm{phytoplankton}}/R_{\mathrm{seawater}}$ and $R = {}^{114}$Cd/^{110}Cd; Abouchami et al., 2014; Janssen et al., 2017; Sieber, Conway, de Souza, Hassler, et al., 2019; Yang et al., 2018). Outside these areas, where Cd is extremely depleted in surface waters (down to <1 pmol kg^{-1}), an open system steady-state model has been suggested to explain the Cd isotope systematics (Xie et al., 2017), though some studies observed a return to lower δ^{114}Cd values at the surface (George et al., 2019; Sieber, Conway, de Souza, Obata, et al., 2019; Xie et al., 2017). At high latitudes, in the Southern Ocean and the subarctic North Pacific, elevated δ^{114}Cd values are restricted to the upper ocean (Abouchami et al., 2014; Janssen et al., 2017; Sieber, Conway, de Souza, Hassler, et al., 2019; Yang et al., 2018). At lower latitudes, where southern-sourced intermediate water masses are present, elevated δ^{114}Cd signals extend down to intermediate depths (∼1,500 m; e.g., Conway & John, 2015a; Sieber, Conway, de Souza, Obata, et al., 2019; Xie et al., 2017), associated with preformed signatures originating in the surface Southern Ocean (Abouchami et al., 2014; Sieber, Conway, de Souza, Hassler, et al., 2019). With the exception of Cd-poor North Atlantic Deep Water (NADW, +0.4‰ to +0.5‰), the global deep ocean exhibits homogeneous δ^{114}Cd (∼+0.25‰; e.g., Abouchami et al., 2014; Conway & John, 2015a; Janssen et al., 2017; John et al., 2018; Sieber, Conway, de Souza, Obata, et al., 2019; Xie et al., 2017; Yang et al., 2018).

While we have a good understanding of the first-order controls of the global Cd and δ^{114}Cd distributions, data in the North Pacific remain very sparse (Conway & John, 2015b; Janssen et al., 2017; Yang et al., 2018), despite it being the location of some of the pioneering Cd studies (Boyle et al., 1976; Bruland, 1980). Here, we present dissolved Cd and δ^{114}Cd data from the US GEOTRACES meridional GP15 transect along 152°W from the Alaskan shelf to the equatorial Pacific. Our goal was to examine controls on Cd biogeochemistry by linking Cd and macronutrient concentrations with Cd isotope ratios in the context of external sources, Southern Ocean and water mass mixing control and internal biological cycling.

2. Methods

2.1. Oceanographic Setting

The GP15 meridional transect traverses from the Alaskan coast (56°N) through the Alaskan Gyre, the North Pacific subtropical gyre, the strongly zonal circulation of the equatorial Pacific to the South Pacific subtropical gyre (20°S, Figure 1). Surface waters of GP15 are intercepted by several regions of strong zonal flow associated with ocean gyre circulation. At its northernmost extent along the Aleutian Islands, the southwestward flowing Alaskan Stream forms the western boundary current of the North Pacific subarctic gyre (Favorite & Ingraham, 1977). A bit further south (∼42°N), the Subarctic Frontal Zone separates the subtropical and subpolar
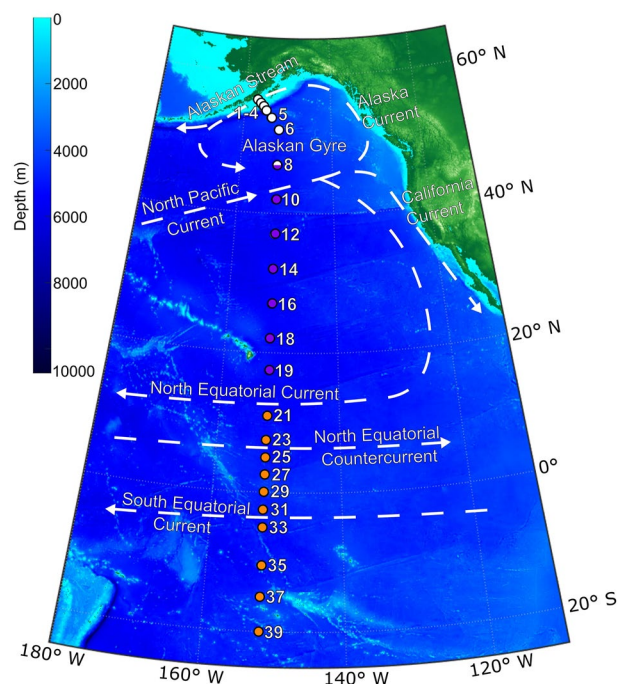
Figure 1. *GP15 cruise track*. Bathymetric map of the North Pacific showing the stations from which samples were collected during the GP15 cruise. Stations are color coded for the North Pacific high-nutrient low-chlorophyll region (white), North Pacific subtropical gyre (purple), and equatorial Pacific and South Pacific subtropical gyre (orange). White dashed arrows represent the major surface circulation.

gyres and is embedded in the broad North Pacific Current that flows eastward on the northern side of the North Pacific subtropical gyre (Roden, 1975). On the south side of the subtropical gyre is the westward North Equatorial Current (∼10°N), which is also one of the three major zonal surface currents in the equatorial Pacific (Talley et al., 2011). Finally, the eastward North Equatorial Countercurrent centered around 5°N and the westward South Equatorial Current complete the equatorial current system and dominate the circulation at the southern end of GP15.

We follow the description of the structure of Pacific water masses by Talley et al. (2011) as the basis of water-mass distributions along GP15. Briefly, the abyssal Pacific contains two water masses: Lower Circumpolar Deep Water (LCDW) and Pacific Deep Water (PDW; Figure 2). Lower Circumpolar Deep Water originates in the Southern Ocean, whereas PDW is formed internally in the North Pacific through diapycnal transformation of deep southern-sourced waters (Talley et al., 2011). Above, at intermediate depths, two low-salinity water masses dominate the Pacific, North Pacific Intermediate Water (NPIW) and Antarctic Intermediate Water (AAIW, Figure 2), which originate at the sea surface of the subarctic and subantarctic latitudes, respectively (Sallée et al., 2010; You, 2003). In the upper ocean the water mass structure is more complex, especially in the tropical Pacific, with different water masses over-lying the intermediate water masses at different latitudes. In the Alaskan Gyre, Pacific Subarctic Upper Water is the main water mass in the upper 200 m, while North and South Pacific Central Water (NPCW/SPCW) make up the thermocline in the subtropics of the North and South Pacific, respec-tively, and span a large range of temperature and salinity (Talley et al., 2011). Equatorward, Subtropical Underwater results from the subduction of surface waters in the center of the subtropical gyre of both hemispheres and can be identified as a shallow salinity maximum (down to 200 m).

2.2. Seawater Sampling

Seawater samples were collected during the US GEOTRACES GP15 section cruise on board the R/V *Roger Revelle* during September–November 2018. On a meridional transect along 152°W from Alaska to Tahiti, 23 stations were sampled for dissolved Cd and δ^{114}Cd (Figure 1). Seawater samples were collected using the GEOTRACES trace-metal clean sampling system (rosette with 24 12 L GO-FLO bottles) or a towfish for surface samples (Cutter & Bruland, 2012). Samples were filtered through acid-cleaned AcroPak capsule filters (0.2 μm) into acid-cleaned LDPE bottles. For Cd concentration and δ^{114}Cd analysis at the University of South Florida (USF), 2 L of filtered seawater were collected, acidified ashore at USF by addition of 2.4 mL 10 M Teflon-distilled HCl, and stored for at least 12 months at pH ∼2 before processing. For Cd concentration analysis at Texas A&M University (TAMU), 250 mL of filtered seawater were collected, acidified shipboard to 0.024 M Optima grade HCl (Fisher Scientific), and stored for at least 3 months (Jensen et al., 2020). For dissolved Cd concentration analysis at the University of Southern California (USC), 1 L of filtered seawater was collected, acidified to pH ∼2 ashore at USC by the addition of 1 mL 12 M Teflon-distilled HCl, and stored for at least 6 months before processing.

2.3. Aerosol Sampling and Processing

Aerosol samples were also collected from 22 deployments of the GP15 cruise using a high-volume sampler and acid-washed 47 mm Whatman 41 ashless, cellulose filters mounted in polypropylene filter holders (Marsay et al., 2022). Filters were then processed shipboard to obtain the soluble Cd fraction extractable in ultrapure water. This fraction was collected by leaching filters on a Savillex fluoropolymer filter holder under vacuum. Over the course of approximately 10 s, 100 mL of ultrapure water was passed through the sample filter and a 0.2 μm polycarbonate backing filter (Buck et al., 2013). Following the extraction of the soluble fraction, 6 M HCl was added to acidify the solution to 0.024 M HCl, and samples were stored for at least a year prior to analysis for soluble Cd and δ^{114}Cd. The soluble aerosol fractions from 11 deployments along the GP15 section were made
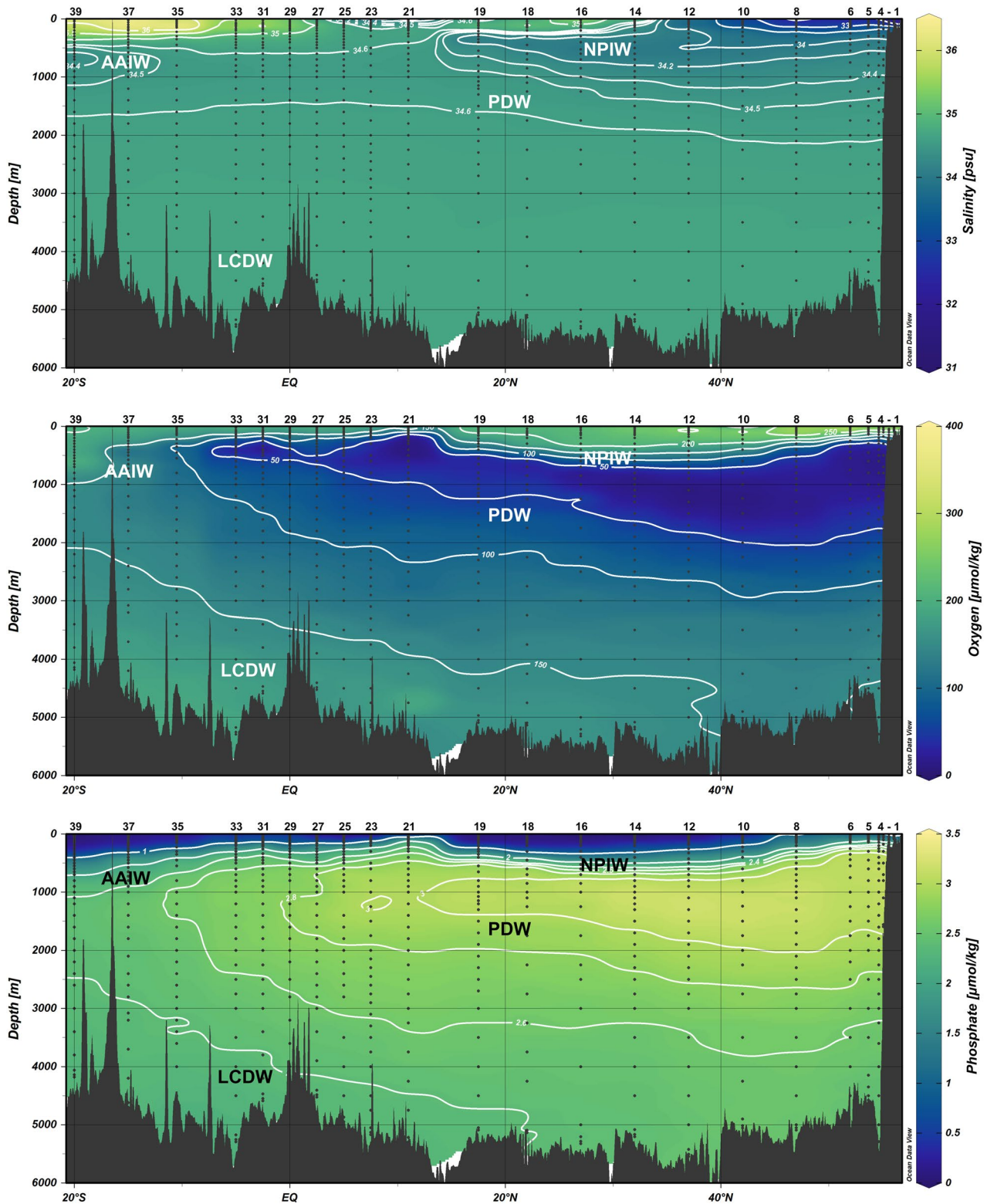
Figure 2. *GP15 salinity, oxygen, and phosphate*. Salinity (top), dissolved oxygen (middle), and dissolved phosphate (bottom) are shown along the GP15 transect. Major water masses based on Talley et al. (2011) are indicated in each section.

Table 1
Aerosol Cd Concentration and Isotope Data

Aerosol deployment	Latitude (°N)	Longitude (°W)	Total aerosol Cd (pmol m^{-3})	Soluble aerosol Cd (pmol m^{-3})	Soluble aerosol δ^{114}Cd (‰)	2SD (‰)	Cd enrichment factor
Aer01	50.01	129.04	0.07	0.02	−0.67	0.59	n.d.
Aer03	55.08	155.72	0.01	0.01	n.d.	n.d.	n.d.
Aer05	52.00	152.00	0.06	0.05	−0.31	0.14	724
Aer07	44.50	152.00	0.27	0.07	−0.33	0.15	1,654
Aer09	37.00	152.00	0.03	0.01	−0.52	0.43	263
Aer11	32.00	152.00	0.03	0.01	−1.05	0.40	2,687
Aer13	18.75	154.90	0.04	0.02	−1.08	0.26	1,095
Aer15	11.00	152.00	0.11	0.11	−0.19	0.12	4,610
Aer17	4.99	152.00	0.10	0.03	−0.38	0.19	10,775
Aer19	−1.12	152.00	0.01	0.02	−0.07	0.25	1,061
Aer21	−10.50	152.00	0.02	0.01	−1.91	0.39	852
Aer23	−20.00	152.00	0.09	n.d.	n.d.	n.d.	6,803

Note. Cd enrichment factors are calculated relative to aerosol Ti (Marsay et al., 2022) and the average crustal Cd/Ti ratio (Rudnick & Gao, 2013). For detailed aerosol sample deployment and recovery information we refer the reader to Marsay et al. (2022).

available for this work (Table 1) and were processed and analyzed for Cd and δ^{114}Cd as described for seawater samples below (Section 2.4).

Additional filters from these aerosol collections were digested at Skidaway Institute of Oceanography and splits of the digested solution were sent to USF for analysis. Marsay et al. (2022) described the digestion procedure which includes three sequential steps aided by heating to 140°C on a hotplate: (a) 1,000 µL concentrated double-distilled nitric acid (d-HNO$_3$); (b) 500 µL concentrated d-HNO$_3$ with 100 µL concentrated hydrofluoric acid (Fisher Trace Metal Grade) and 100 µL concentrated hydrogen peroxide (Fisher Optima Grade); (c) 500 µL concentrated d-HNO$_3$. Each heating step was conducted overnight, with samples taken to dryness the following day. Following the third dry-down, residues were dissolved in 0.32 M d-HNO$_3$ for analysis. The digested filter fractions from 11 deployments along the GP15 section were made available for this work (Table 1). Samples were purified by anion-exchange chromatography but did not require extraction using Nobias PA-1 chelating resin prior to Cd and δ^{114}Cd analysis as described for seawater samples below (Section 2.4).

2.4. Cd Concentration and Isotope Analysis

Discrete aliquots of filtered seawater samples from the same GO-FLO bottles were subsampled shipboard into separate bottles for USF (2–4 L), Texas A&M (250 mL), and USC (1 L) and then analyzed back on shore by each respective lab, providing three independent analyses of Cd concentration in the GP15 samples. Cd isotope ratios (δ^{114}Cd) were measured only in USF's samples. A brief description of the methods used by the three groups follows.

2.4.1. University of South Florida

Seawater samples were processed for isotope analysis following Sieber, Conway, de Souza, Obata, et al. (2019). Briefly, a ^{111}Cd–^{113}Cd double-spike was added prior to the batch extraction using Nobias PA-1 chelating resin, followed by purification by anion-exchange chromatography using AG-MP1 resin. The method has a procedural blank of <1 pg. Cadmium isotope analyses were performed on a Thermo Neptune Plus MC-ICPMS in the Tampa Bay Plasma Facility at USF using an Apex-Q introduction system. We express Cd stable isotope ratios in delta notation relative to the NIST SRM-3108 Cd standard:

$$\delta^{114/110}\text{Cd} = \left[\frac{(^{114}\text{Cd}/^{110}\text{Cd})_{\text{sample}}}{(^{114}\text{Cd}/^{110}\text{Cd})_{\text{NIST SRM−3108}}} - 1 \right] \times 1000$$

A secondary standard, BAM-I012, was analyzed over eight sessions on the same timescale as the samples to provide an estimate of long-term instrumental precision. We obtain a value of $-1.32‰ \pm 0.06‰$ (2SD, $n = 172$), in agreement with consensus values (Abouchami et al., 2013). Using the 2SD of offsets from the mean of full replicate measurements based on 26 pairs of replicate analysis on separate seawater samples collected at the same depth (the GP15 sampling strategy collected overlapping samples between casts, Table S1), we obtain a second estimate of external precision (0.05‰), which is similar to analytical precision. Therefore, we consider a 2SD uncertainty of 0.06‰ as a conservative estimate of analytical precision and have applied it to all samples, except for low concentration samples where the larger internal error is considered a more conservative estimate of uncertainty. Concentrations were calculated using the isotope dilution technique based on on-peak blank, interference, and mass-bias corrected $^{114}Cd/^{111}Cd$ ratios measured simultaneously with isotope analyses (Sieber, Conway, de Souza, Obata, et al., 2019). We express uncertainty (1SD) on Cd concentrations as 2%, based on replicate analysis of separate seawater samples collected at the same depth ($n = 26$).

2.4.2. Texas A&M University

Dissolved Cd concentrations were measured at TAMU under low-particle conditions using an automated flow-injection technique adapted for a SeaFAST pico offline ICP-MS method (Jensen et al., 2020; Lagerström et al., 2013). Briefly, samples were spiked with ^{111}Cd, buffered inline with precleaned ammonium acetate to a pH of 6.2 ± 0.2 immediately prior to loading onto a column filled with Nobias PA-1 resin, and finally back-eluted with 10% (v/v) optima grade HNO_3 (Fisher Scientific). Subsequently, samples were analyzed on a Thermo Element XR HR-ICPMS at the TAMU R. Ken Williams Radiogenic Laboratory, and Cd concentrations were calculated via isotope dilution. We express uncertainty (1SD) on Cd concentrations as 2%, based on replicate analysis of separate seawater samples collected at the same depth ($n = 26$).

2.4.3. University of Southern California

Dissolved Cd concentrations were measured at USC using a seaFAST pico offline system (Lagerström et al., 2013). Briefly, samples were spiked with ^{110}Cd, loaded onto a Nobias PA-1 resin column, and eluted with 1M Teflon-distilled HNO_3 (Aristar Ultra™). Subsequently, samples were analyzed on a Thermo Element 2 HR-ICPMS at USC, and Cd concentrations were calculated via isotope dilution. We express uncertainty (1SD) on Cd concentrations as 3%, based on replicate analysis of separate seawater samples collected at the same depth ($n = 17$).

2.4.4. Intercomparison Between Groups, a Synthesized Data Product, and Error Estimation

We show excellent agreement between the three laboratories for dissolved Cd concentrations over the whole range of concentrations measured for GP15 samples (Figure S1 in Supporting Information S1). For figures and discussion in this paper, we therefore use a combined GP15 Cd concentration data product, calculated as the mean of Cd concentrations from all three groups at each bottle depth, except for obvious outliers (excluded from average calculations), samples which were not measured by all three groups, or at surface depths where the 4 L samples measured by USF provide better accuracy. The error on GP15 Cd concentrations in this combined data set is calculated as the 1SD on the mean from all three labs (4%), although each lab also describes individual uncertainty.

2.5. Phosphate Analyses and Cd*

Phosphate analyses were performed using the Oceanographic Data Facility on a Seal Analytical continuous-flow AutoAnalyzer 3 following a method modified from Bernhardt and Wilhelms (1967). Briefly, acidified ammonium molybdate was added to a seawater sample to produce phosphomolybdic acid, which was then reduced to colored phosphomolybdous acid by addition of dihydrazine sulfate. Subsequently, the sample was passed through a 10 mm flow cell and absorbance measured at 820 nm. We assign an error (1SD) of 0.019 μmol/kg based on repeat measurements of reference materials for seawater.

We calculated Cd* following Janssen et al. (2014). This calculation was based on measured Cd and PO_4 concentrations in this study, using the deep North Pacific $Cd:PO_4$ ratio as a reference point (0.35 mmol mol^{-1}). To assess the propagated uncertainty in Cd*, we use the reported 1SD uncertainties on PO_4 (± 0.019 μmol kg^{-1}) in combination with the 1SD uncertainties on Cd (± 0.016 nmol kg^{-1}) based on their interlaboratory reproducibility to obtain a conservative estimate of the maximum-propagated uncertainty (1SD) of ± 0.023 nmol kg^{-1} for Cd*.

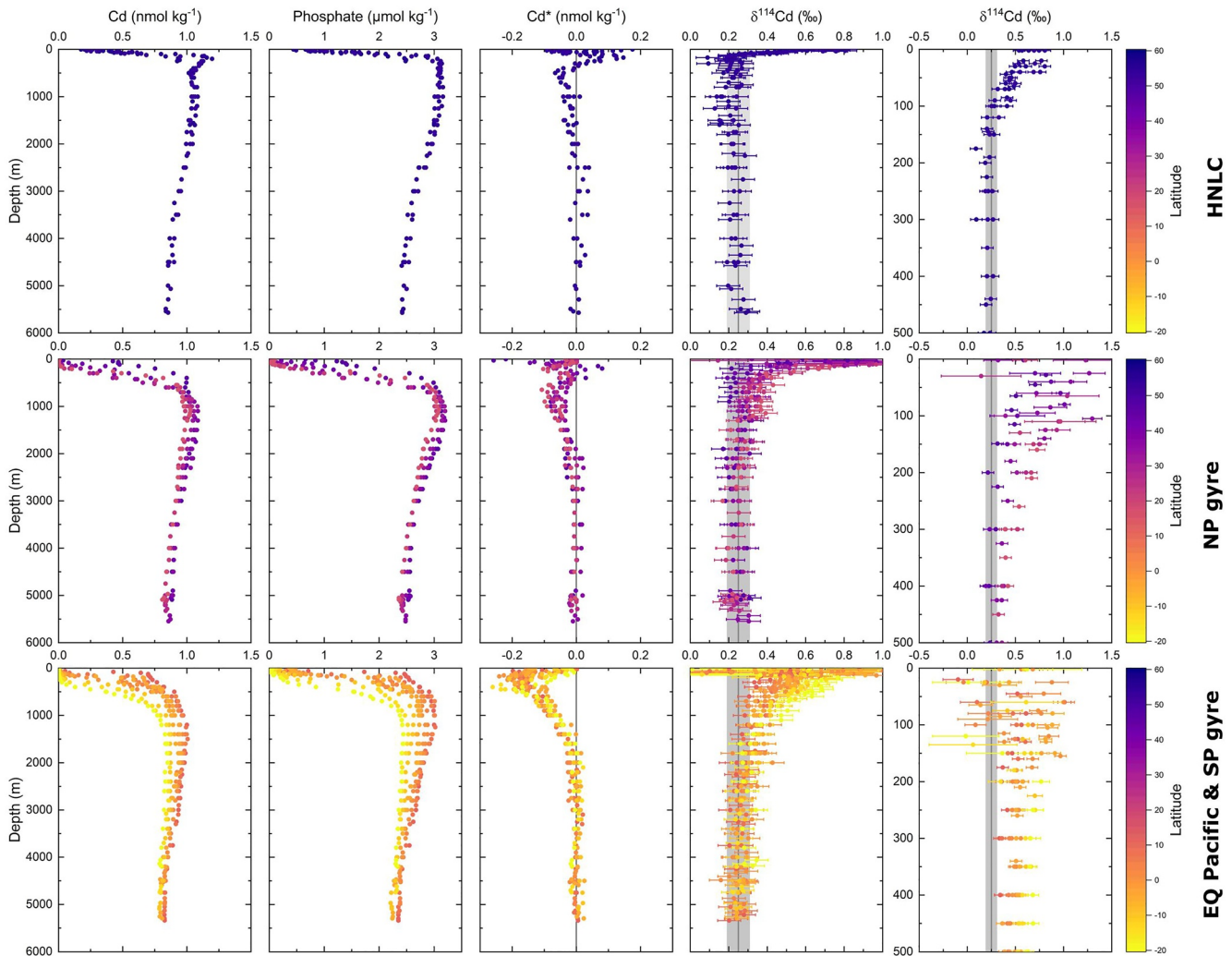**Figure 3.** *GP15 water column profiles*. Dissolved Cd concentration, Cd isotope ratios (δ^{114}Cd), phosphate, and Cd* for the North Pacific high-nutrient low-chlorophyll region (stations 1–6), the North Pacific subtropical gyre (stations 8–19), and the equatorial Pacific and South Pacific subtropical gyre (stations 21–39). The far-right column shows a zoom in on the upper 500 m for δ^{114}Cd. The gray bar denotes the deep ocean δ^{114}Cd average ($+0.25‰ \pm 0.06‰$).

3. Results

Dissolved Cd concentrations along the transect range over four orders of magnitude, between 0.5 pmol kg^{-1} and 1.19 nmol kg^{-1}, with Cd at its most depleted in surface waters and showing a general increase with depth, confirming its nutrient-type distribution (Figures 3 and 4). Concentration profiles of stations located in the North Pacific HNLC region (1–6, Figure 1) are distinctly different from those further south (Figure 3) with a less pronounced surface depletion ($\sim$0.2–0.3 nmol kg^{-1}) and a shallow subsurface maximum (up to $\sim$1.2 nmol kg^{-1} at $\sim$200 m). Stations located in the North Pacific subtropical gyre (10–19, Figure 1) exhibit extremely low surface Cd ($<$0.01 nmol kg^{-1}) and a deeper Cd maximum at depths around 1,000 m (Figures 3 and 4), with station 8 representing the transition from HNLC to the gyre. While the Cd maximum deepens ($\sim$1,500 m) and surface Cd remains low in the equatorial Pacific (stations 21–33, Figure 1), subsurface Cd concentrations (50–400 m) increase (Figures 3 and 4). At the southern end of GP15 (stations 35–39), in the South Pacific subtropical gyre, subsurface Cd concentrations decrease again and the Cd maximum occurs at greater depths ($\sim$2,000 m, Figures 3 and 4). At depths below 2,000 m, Cd concentrations are relatively homogeneous regardless of the upper ocean regime, showing a slight decrease with depth within a profile and a decrease southward along the transect.

Dissolved δ^{114}Cd range between $-0.1‰$ and $+1.3‰$, generally decrease with depth and exhibit an inverse relationship with Cd concentrations (Figures 3 and 4). Overall, dissolved δ^{114}Cd shows little variability in the deep
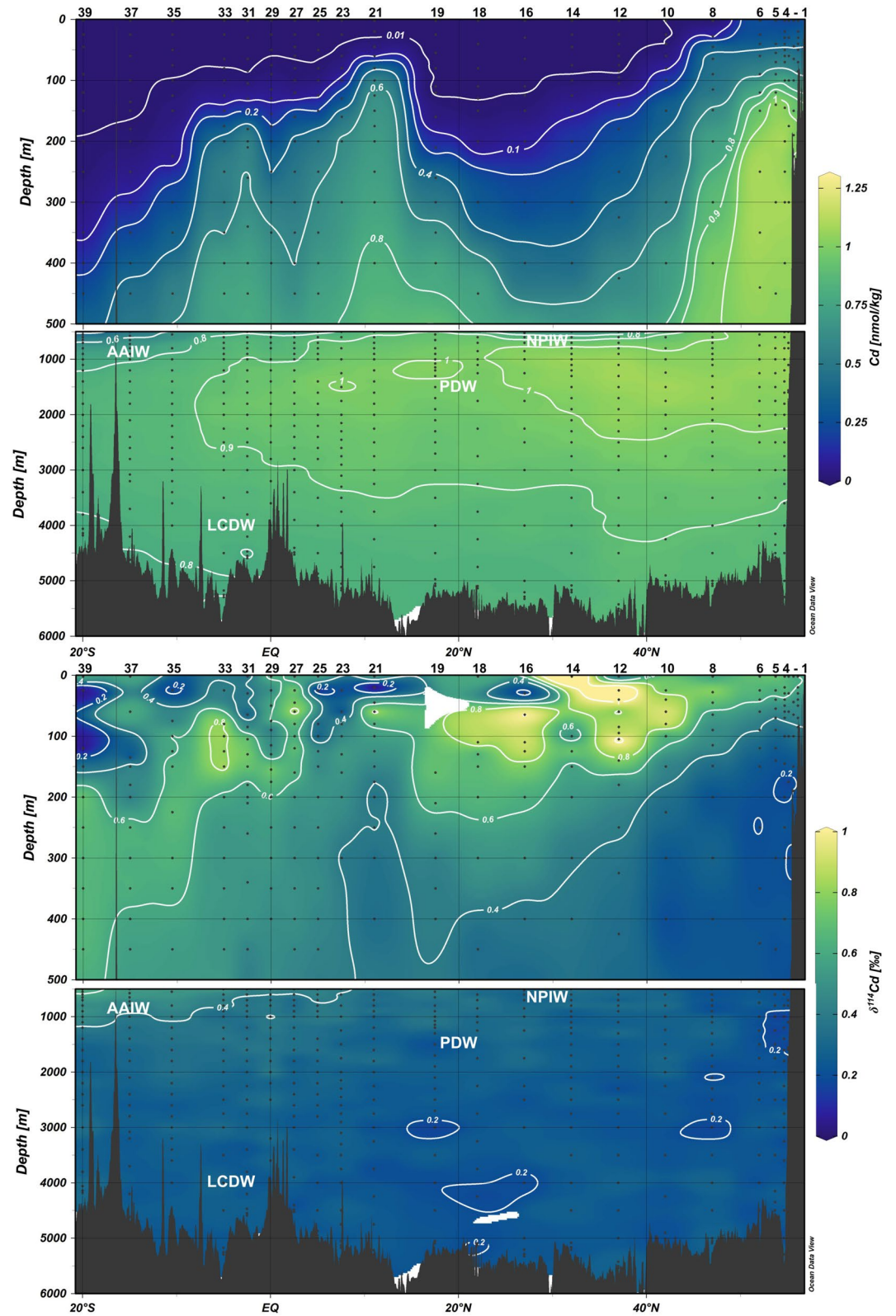
Figure 4. *GP15 section Cd data*. Dissolved Cd concentration (top) and dissolved δ^{114}Cd (bottom) along the GP15 transect. The upper (0–500 m) and deep ocean (500–6,000 m) are shown in separate panels on different depth scales.

ocean (below 2,000 m, +0.25‰ ± 0.06‰ 2SD, n = 203) and an increase to higher values in the upper ocean (top 1,000 m). As noted above for Cd concentrations, the δ^{114}Cd profiles for stations in the North Pacific HNLC region (stations 1–6) are notably different from the rest of the section, in that the δ^{114}Cd maximum is at the surface (+0.5‰ to +0.8‰) with constant δ^{114}Cd below ~200 m (+0.25‰). In the North Pacific subtropical gyre (stations 10–19), δ^{114}Cd values are slightly elevated (~+0.30‰) at intermediate depths (500–1,000 m), coinciding with the salinity minimum. A similar signal of elevated δ^{114}Cd (+0.4‰ to +0.5‰) also occurs in intermediate waters of the equatorial Pacific (stations 21–33) and intensifies (up to +0.7‰) in the South Pacific subtropical gyre (stations 35–39) as Cd concentrations decrease. At shallow depths (top 100 m), in the extremely Cd-depleted surface waters (stations 8–39), δ^{114}Cd values are highly variable, continuing to increase to >1‰ in some places, while decreasing as low as −0.1‰ in others (Figures 3 and 4).

The distribution of dissolved PO_4 along the GP15 transect is overall very similar to Cd, exhibiting similar features as described above for Cd concentrations. We use Cd* to highlight the differences between the distributions of the two elements. Cd* ranges from −0.32 to +0.18 nmol kg^{-1}, with the strongest Cd* signals restricted to the upper ocean (top 500 m), and a constant Cd* of ~0 nmol kg^{-1} below 2,000 m (Figure 3). In the North Pacific HNLC region (stations 1–6), a Cd* maximum in the shallow subsurface (~200 m) is overlain by negative Cd* in surface waters, except for stations on the Alaskan shelf (stations 1–2) where Cd* is >0 nmol kg^{-1} at the surface (Figure 3). Across the northern subtropical gyre (stations 10–19), there is a slight Cd deficit relative to PO_4 in the subsurface (100–300 m), reflected in negative Cd* values (~−0.07 nmol kg^{-1}). Below, coinciding with the salinity minimum (~500 m), Cd* increases to ~0 nmol kg^{-1} (Figure 3). In the equatorial Pacific and the South Pacific subtropical gyre (stations 21–39), the negative Cd* signal in the upper ocean intensifies (−0.3 to −0.1 nmol kg^{-1}) and exhibits a minimum around 200–400 m depth. Contrary to the North Pacific subtropical gyre, Cd* remains negative in the underlying intermediate waters (−0.15 to −0.05 nmol kg^{-1}, 500–1,000 m; Figure 3). Below these upper ocean features, Cd* exhibits a deeper minimum (−0.05 nmol kg^{-1}) centered around 1,000 m across the entire section that wanes with depth returning to ~0 nmol kg^{-1} between 1,500 and 2,000 m (Figure 3).

Total and soluble aerosol Cd concentrations measured along the GP15 range from 0.01 to 0.27 pmol m^{-3} and from 0.01 to 0.11 pmol^{-3}, respectively (Table 1). Cadmium isotope compositions in the soluble aerosol fraction are light, ranging between −1.91‰ and −0.07‰ (Table 1). Both, aerosol Cd concentrations and isotope compositions show no latitudinal pattern along the transect.

4. Discussion

4.1. Influences on Cd Signatures in the Upper Ocean (Top 300 m)

Surface waters along GP15 in the North Pacific HNLC (stations 1–6) exhibit elevated Cd concentrations, consistent with the supply of nutrient-rich waters from below, followed by a shallow subsurface Cd maximum at ~200 m. Surface HNLC waters (<100 m) also show negative Cd* values indicating preferential uptake of Cd relative to PO_4, while the subsurface maximum is associated with positive Cd* values as a consequence of regeneration of this "excess" Cd (Figure 3), analogous to what has been proposed for Zn (Vance et al., 2019). This pattern of increased Cd uptake and very shallow regeneration has been observed previously in HNLC regions (Baars et al., 2014; Janssen et al., 2017; Sieber, Conway, de Souza, Hassler, et al., 2019; Yang et al., 2018) and appears to be the typical behavior of Cd under HNLC conditions in the absence of external influences. The Cd isotope systematics (Figure 5a) also show a similar pattern observed previously under HNLC conditions, following a closed system Rayleigh fractionation driven by biological uptake with α = 0.99965 (0.9993–0.9999, Abouchami et al., 2014; Janssen et al., 2017; Sieber, Conway, de Souza, Hassler, et al., 2019; Yang et al., 2018).

Of the HNLC stations along GP15, only surface waters at station 1 on the Alaskan shelf show small deviations from the Cd concentration and Cd* pattern, with slightly higher surface Cd concentrations (0.33 nmol kg^{-1}) and elevated Cd* (0.18 nmol kg^{-1}); these are the depths also associated with the lowest salinity observed along GP15, as low as 31.4, indicating potential riverine influence from the Alaska Coastal Current. However, surface δ^{114}Cd show no deviations from the isotope systematics driven by biological uptake as described above (Figure 5a). Therefore, rather than input from a riverine source, these anomalies likely reflect weakened Cd uptake relative to phosphate due to elevated trace metals such as Fe and Mn in nearshore waters. The only deviations from uptake-driven closed system Rayleigh systematics occurred in the surface waters of stations 2 and 3, exhibiting slightly lower δ^{114}Cd values (+0.40‰ to 0.64‰, Figure 5a). Both stations are located within the influence of
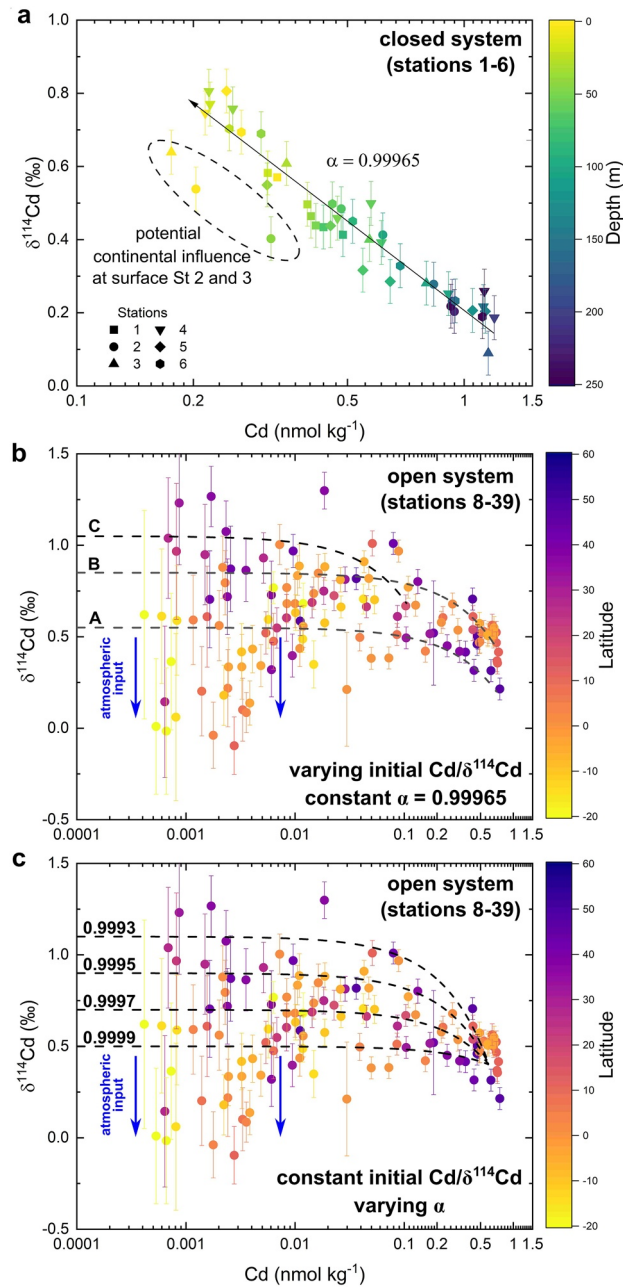
Figure 5. *Cd isotope systematics in the upper ocean (top 300 m).* (a) Stations 1–6 within the North Pacific high-nutrient low-chlorophyll (HNLC) region follow a closed system Rayleigh fractionation trend (fractionation factor $\alpha = 0.99965$, where $\alpha = R_{\text{phytoplankton}}/R_{\text{seawater}}$ and $R = {}^{114}Cd/{}^{110}Cd$). (b, c) Cd isotope systematics for stations outside the HNLC (8–39) can be described using a steady-state open system model (Xie et al., 2017) using different initial Cd compositions with a constant fractionation factor (b) or different fractionation factors with a constant initial Cd composition (c). Initial Cd compositions are chosen to represent the variability of Cd supplied to the surface ocean along the GP15 section ((A) 0.7 nmol kg^{-1}, +0.2‰; (B) 0.5 nmol kg^{-1}, +0.6‰; and (C) 0.1 nmol kg^{-1}, +0.7‰) using $\alpha = 0.99965$ that was derived under HNLC conditions. Fractionation factors represent the range of the previously observed values in the Pacific (Janssen et al., 2017; Sieber, Conway, de Souza, Hassler, et al., 2019; Yang et al., 2018) using an averaged initial Cd composition (0.6 nmol kg^{-1}, +0.4‰). Atmospheric inputs can shift δ^{114}Cd to lower values at extremely low Cd concentrations (blue arrows).

the Alaskan Stream (salinity ~32.2), which could also carry a small amount of Cd from continental sources with a near-crustal δ^{114}Cd signature (~+0.1‰, Lambelet et al., 2013). A lateral input of isotopically light Cd could affect δ^{114}Cd surface signatures, causing them to deviate from the biologically driven HNLC relationship (Figure 5a).

Outside the North Pacific HNLC region (stations 8–39), upper-ocean waters exhibit extreme Cd-depletion (down to <1 pmol kg^{-1}), extending down to depths of 200 m in the subtropics of the North and South Pacific associated with NPCW and SPCW, respectively. Cd isotope systematics for the upper ocean are distinctly different from HNLC waters, but GP15 data exhibit a similar upper ocean trend to recent studies in the Pacific (George et al., 2019; Janssen et al., 2017; Sieber, Conway, de Souza, Obata, et al., 2019; Yang et al., 2018). However, along GP15 surface δ^{114}Cd only increase to 1.3‰ under extreme Cd-depletion, while other studies have found δ^{114}Cd >1.5‰ in the northern gyres of both the Atlantic and Pacific Oceans (Conway & John, 2015b; John et al., 2018; Ripperger & Rehkämper, 2007; Xue et al., 2012), including surface samples collected at the SAFe station, located ~1,000 km east of GP15 station 14 (Conway & John, 2015b). While the observation of δ^{114}Cd up to +1.5‰ at depleted Cd concentrations has been reported by multiple laboratories using multiple analytical techniques, the accuracy of more heavily enriched compositions has remained under debate since they have only been reported by multicollector ICPMS using a ^{110}Cd–^{111}Cd double spike and not repeated by TIMS or multicollector ICPMS techniques using a ^{111}Cd–^{113}Cd double spike (Janssen et al., 2017; Sieber, Conway, de Souza, Obata, et al., 2019). While we cannot rule out a natural source for these previously reported high δ^{114}Cd values (e.g., species variability or overprinting by aerosol deposition), their absence (Figure 4) in our large surface data set (at the same location and season as from previous studies) does lend weight to the suggestion that these may be the result of an unknown analytical artifact, perhaps relating specifically to interferences on the ^{110}Cd beam.

Instead, the upper ocean Cd isotope systematics along GP15 can be described using a steady state open system model (Figure 5, Xie et al., 2017), which reflects the overall trend in the observed data and can account for the lack of high δ^{114}Cd in extremely Cd-depleted waters. Figure 5b shows that most of the data can be explained using an open system model with the fractionation factor derived in the North Pacific HNLC region (α = 0.99965) and variable upwelled initial Cd compositions along the transect. Initial Cd compositions are chosen to represent the variability of Cd supplied to the surface ocean based on subsurface Cd compositions along the GP15 section. However, the variation of the fractionation factor within a range consistent with previous observations in the Pacific (α = 0.9993–0.9999, Janssen et al., 2017; Sieber, Conway, de Souza, Hassler, et al., 2019; Yang et al., 2018) and a constant initial Cd composition can produce a similar range of surface δ^{114}Cd (Figure 5c). Both factors likely contribute to the changing surface Cd signatures as the biogeochemical setting changes along the GP15 transect.

However, an open system model cannot explain the shift toward lighter isotope compositions at very low Cd concentrations (Figure 5), analogous to observations in the South Pacific (George et al., 2019). Previous studies have suggested that this reversal toward lower δ^{114}Cd values in surface waters could be caused by supply limited Cd uptake (Gault-Ringold et al., 2012), binding of Cd by organic ligands (Xie et al., 2017), atmospheric inputs of anthropogenic Cd (Bridgestock et al., 2017), or a combination of these processes (George et al., 2019). Under supply limited conditions, phytoplankton would utilize all Cd that is available, resulting in no net isotopic fractionation during uptake (Gault-Ringold et al., 2012). At the lowest Cd concentrations, it may also be possible that ligand-bound Cd constitutes the majority of dissolved Cd, buffering surface δ^{114}Cd to relatively low values (Xie et al., 2017). However, both cases can only explain a reversal of surface δ^{114}Cd to the composition of upwelled waters, which is always heavier (≥+0.2‰) than the observed δ^{114}Cd in surface waters along GP15 (down to −0.1‰). Therefore, neither of the two models can account for the shift toward lighter isotope compositions at very low Cd concentrations, suggesting that atmospheric inputs play an important role in setting surface δ^{114}Cd.

Cadmium enrichment factors of aerosols collected along GP15, calculated using aerosol Ti data from Marsay et al. (2022) and an average crustal Cd/Ti ratio (Rudnick & Gao, 2013), are highly elevated (263–10,775, Table 1). Cadmium isotope compositions in the soluble aerosol fraction (−1.91‰ to −0.07‰, Table 1) exhibit a similar range as anthropogenic Cd aerosols, where light isotope compositions are driven by large Cd isotope fractionations that can be produced by evaporation (−1.6‰ to +0.8‰; e.g., Bridgestock et al., 2017; Cloquet et al., 2006; Rehkämper et al., 2012). Together, the consistently light Cd isotope compositions in the soluble aerosol fraction and the high Cd enrichment factors in aerosols are strong indicators that anthropogenic Cd is the dominant component in aerosols delivered to surface waters of the North Pacific (e.g., Zhong et al., 2020), at least during the low dust season at this time of the year. Therefore, we suggest atmospheric inputs carrying isotopically light Cd of anthropogenic origin as the main cause of lower surface δ^{114}Cd values along GP15 (Figure 5). Using a mean bulk deposition velocity of 1,764 m d^{-1} for stations outside the Intertropical Convergence Zone (ITCZ) and 4,570 m d^{-1} for Aer15 located within the ITCZ (Marsay et al., 2022), we calculated bulk and soluble deposition fluxes of aerosol Cd both in the range of 0.02–0.50 nmol m^{-2} d^{-1}. Outside the major
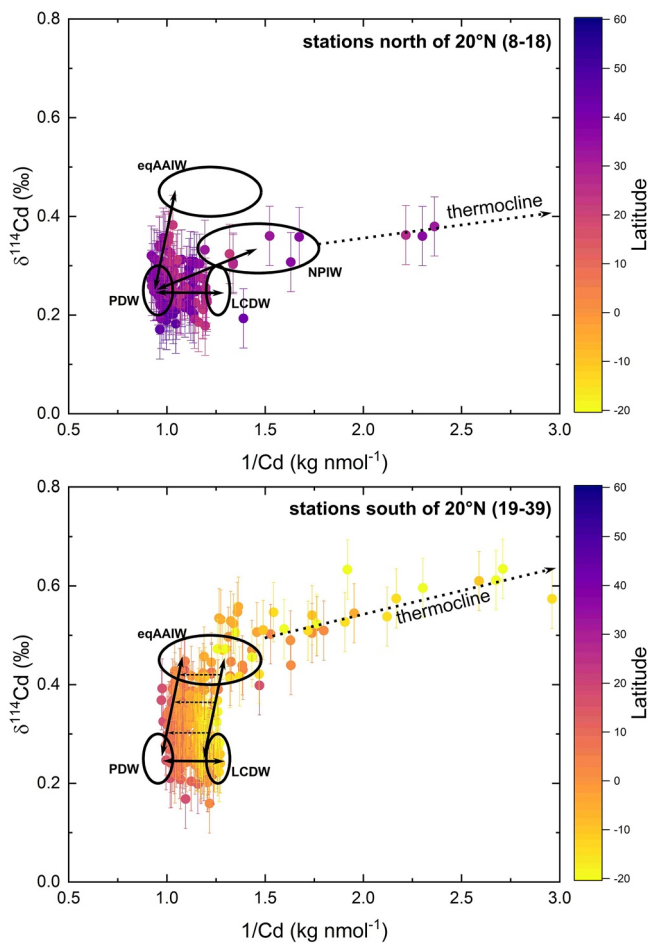
Figure 6. *Isotope mixing of subsurface water mass endmembers along GP15.* Figure includes all data below 300 m for stations located north of 20°N (top, stations 8–18, North Pacific Intermediate Water-dominated), and stations located south of 20°N (bottom, stations 19–39, Antarctic Intermediate Water [AAIW]-dominated). Stations 1–6 located within the North Pacific high-nutrient low-chlorophyll region where 1D-cycling is dominating Cd systematics are not shown here. All data fall on mixing lines (black arrows) between the water mass endmembers (circles). The evolution above intermediate waters toward the seasonal thermocline is shown by the dotted arrow. Dashed arrows indicate the shift of the mixing line between eqAAIW and Pacific Deep Water as Cd concentrations in both water masses increase northward along GP15.

upwelling regions in the North and equatorial Pacific, the soluble deposition flux is on the same order or larger than the upwelling flux of Cd at 100 m (Figure S2 in Supporting Information S1), which, especially given their extremely light isotope compositions, allows atmospheric inputs to modify surface δ^{114}Cd. Furthermore, seasonal physical stratification of the surface ocean in the North Pacific isolates the surface mixed layer from spring to late autumn (Bathen, 1972), likely increasing the impact of atmospheric inputs on extremely Cd-depleted surface waters (Bruland et al., 1994). Together, these factors all point to aerosols of anthropogenic origin playing an important role in setting δ^{114}Cd of low-Cd surface waters in the Pacific. Further studies will be required to assess spatial and seasonal variations of atmospheric deposition fluxes of Cd and determine the impact of atmospheric Cd on surface waters on a global scale.

4.2. Water Mass Mixing Controls on Cd Signatures in Intermediate and Deep Waters

Subsurface dissolved [Cd], Cd*, and δ^{114}Cd have been shown previously to be controlled by water mass mixing of defined water mass endmembers in the Atlantic and South Pacific Oceans (Abouchami et al., 2014; George et al., 2019; Sieber, Conway, de Souza, Obata, et al., 2019; Xie et al., 2017). Here, we extend this approach to the North Pacific, specifically focusing on the shifting influence of northern-sourced NPIW and southern-sourced AAIW at intermediate depths along GP15.

The major formation region of AAIW is in the southeast Pacific where Cd* and δ^{114}Cd signatures are imparted and then conserved into the low latitudes of the South Pacific (-0.1 nmol kg^{-1}, $+0.46‰$, Sieber, Conway, de Souza, Hassler, et al., 2019; Sieber, Conway, de Souza, Obata, et al., 2019). The Cd* and δ^{114}Cd signatures associated with the salinity minimum at the southern-most GP15 stations (-0.1 nmol kg^{-1}, $+0.45‰$ at stations 37, 39), as well as the Cd concentrations ($\sim$0.6 nmol kg^{-1}), agree with these previous observations, confirming that the preformed AAIW δ^{114}Cd signature reaches the latitudes of GP15 (15–20°S) without modification. As AAIW enters the tropics (5–10°S, stations 33 and 35) as equatorial AAIW (eqAAIW), its Cd concentration increases (up to 0.85 nmol kg^{-1}) but it retains its preformed δ^{114}Cd signature as a consequence of equatorial upwelling carrying a δ^{114}Cd that closely matches the preformed signature of AAIW and feeding near-complete consumption in surface waters followed by addition of similarly heavy Cd to eqAAIW via regeneration of organic matter (John et al., 2018; Sieber, Conway, de Souza, Obata, et al., 2019). However, our data show that as eqAAIW crosses the equatorial Pacific and extends into the northern hemisphere, Cd concentrations continue to increase (up to

$\sim$0.9 nmol kg^{-1}) and δ^{114}Cd gradually decreases ($+0.3‰$ to $0.4‰$, stations 31–21). We attribute these changes to a combination of continuous mixing of AAIW with underlying PDW and addition of Cd via regeneration (Figure 6), until AAIW reaches its northern boundary around 15°N. However, while AAIW does not enter the North Pacific subtropical gyre as a salinity minimum, it is nonetheless entrained into the North Pacific (Kawabe & Fujio, 2010). The influence of AAIW on the δ^{114}Cd signatures of North Pacific intermediate waters within the subtropical gyre is evident (Figure 6a), reaching as far north as 47°N (station 8). This observation is in line with recent findings derived from analyses of Nd isotopes, which show a similarly strong impact of AAIW on North Pacific intermediate waters (Fuhr et al., 2021) and emphasizes the importance of Southern Ocean surface processes on the Cd and δ^{114}Cd distributions even in the North Pacific.

On the other hand, the extent of NPIW is restricted to the North Pacific and its influence on the large-scale Cd distributions remains poorly understood due to the dearth of North Pacific data. Recently, Yang et al. (2018)

characterized the source signature of NPIW near its formation region in the Kuroshio-Oyashio extension in the western North Pacific (0.70 nmol kg^{-1}, +0.31‰ ± 0.09‰) showing a slight depletion of Cd relative to PO$_4$, reflected in Cd* (∼–0.05 nmol kg^{-1}). North Pacific Intermediate Water is characterized by the salinity minimum (about 34.0–34.3) and traverses the North Pacific eastwards to reach GP15 as part of the North Pacific Current around ∼42°N (You, 2003). Along GP15, the core of NPIW shows a Cd signature very similar to that of Yang et al. (0.73 nmol kg^{-1}, +0.32‰ ± 0.05‰) and similar Cd* values (−0.05 to 0 nmol kg^{-1}), also consistent with previous observations at SAFe (0.80 nmol kg^{-1}, +0.30‰ ± 0.04‰, −0.07 nmol kg^{-1}; Conway & John, 2015b). This suggests that the source signature of NPIW is conserved as it crosses the North Pacific, analogous to AAIW in the South Pacific (Sieber, Conway, de Souza, Obata, et al., 2019).

Despite a ∼20% change in Cd concentration between 2,000 m and the deepest waters of the North Pacific, deep ocean δ^{114}Cd along GP15 is remarkably homogeneous at depth (+0.25‰ ± 0.06‰, 2SD, n = 203). This arises principally due to the fact that LCDW and PDW are, ultimately, both southern-sourced water masses since PDW is formed internally in the North Pacific and has no surface sources (Talley et al., 2011). Therefore, the concentration difference between the two water masses can be attributed to Cd addition via regeneration as the deep waters circulate through the Pacific. That there is no net change in δ^{114}Cd throughout the deep ocean is partly due to the fact that LCDW already carries relatively high Cd concentrations after formation in the Southern Ocean which allows it to absorb small amounts of variable δ^{114}Cd compositions without a significant change in its δ^{114}Cd signature (Janssen et al., 2017; Sieber, Conway, de Souza, Obata, et al., 2019). Also, regeneration from different biogeochemical settings throughout the Pacific likely contributes organic matter carrying different δ^{114}Cd, resulting in an integrated signal that is similar to the deep water δ^{114}Cd (Sieber, Conway, de Souza, Obata, et al., 2019). As a consequence of this deep ocean δ^{114}Cd homogeneity, regeneration and mixing between PDW and LCDW operate along the same horizontal "line" in Figure 6, driving Cd concentration changes while δ^{114}Cd remains unchanged.

Overall, the subsurface Cd and δ^{114}Cd distribution is described well by mixing water mass endmembers, with data falling on mixing lines between adjacent water masses (Figures 6a and 6b). Water mass endmembers are defined based on T-S characteristics as defined by Talley et al. (2011), and Cd characteristics are assigned based on GP15 data in combination with previous studies (George et al., 2019; Janssen et al., 2017; John et al., 2018; Sieber, Conway, de Souza, Hassler, et al., 2019; Sieber, Conway, de Souza, Obata, et al., 2019). Although δ^{114}Cd signatures of eqAAIW and NPIW are well-constrained, their Cd concentrations vary significantly along GP15 (Figure 6). While Cd concentrations of NPIW can be fairly well constrained at the core of NPIW (∼0.7 nmol kg^{-1},

Yang et al., 2018; this study), the concentration range indicated in Figure 5a is a consequence of the fact that the density range occupied by NPIW exhibits a significant Cd gradient (0.4–0.9 nmol kg^{-1}). As described above, Cd concentrations in eqAAIW span a large range, increasing northward, due to Cd addition via regeneration (Sieber, Conway, de Souza, Obata, et al., 2019). Similar to eqAAIW, Cd concentrations in PDW also increase northward due to regeneration (Janssen et al., 2017). Together, these changes lead to a gradual shift of the mixing line between eqAAIW and PDW toward higher Cd concentrations from the southern to the northern end of the AAIW-dominated part of GP15 (Figure 6).

4.3. Cd-PO$_4$ Relationship and Cd* Anomalies

The Cd-PO$_4$ relationship for data from GP15 (Figure 7) fits into the framework of Cd-PO$_4$ systematics of the Pacific described by Sieber, Conway, de Souza, Obata, et al. (2019). The majority of the data fall on two Southern-Ocean-determined slopes, with surface waters forming the shallow slope and intermediate and deep water the steep slope. The upper ocean in the North Pacific HNLC region does not follow this trend as regional cycling processes play a more important role here (Section 4.1). While Southern Ocean processes in combination with water mass formation and mixing can account for the large-scale relationship between Cd and PO$_4$, Figure 7 also highlights
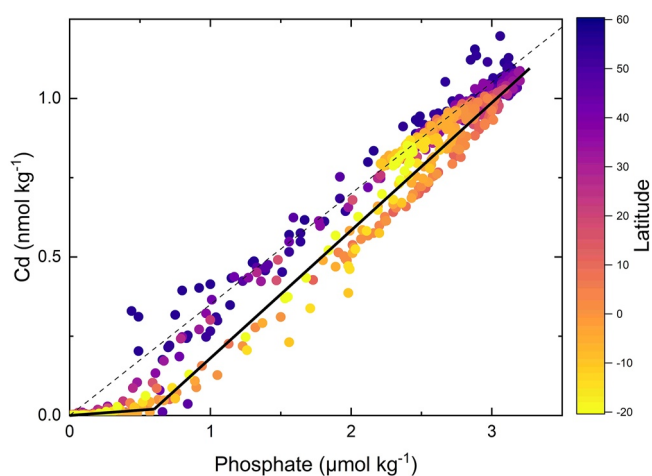

Figure 7. *Dissolved Cd-PO$_4$ relationship for data from GP15*. Solid lines represent the determined slopes, with surface waters forming the shallow slope and intermediate and deep water the steep slope (Sieber, Conway, de Souza, Hassler, et al., 2019). The dashed line represents a Cd* of 0 nmol kg^{-1} using a Cd:PO$_4$ of 0.35 mmol mol^{-1}.

deviations from this correlation, which are reflected in Cd*. Below we investigate the Cd* anomalies along GP15 within the framework of Southern-Ocean-driven Cd-PO$_4$ systematics.

Waters at depths of 700–1,500 m along the entire section show a deeper Cd* minimum centered around 1,000 m (~–0.05 nmol kg^{-1}, Figures 3 and 8) indicative of a slight Cd deficit relative to PO$_4$ compared to the underlying deep ocean. Only at the northern end of GP15, in the HNLC region, does this signal shoal slightly to ~500 m. Here, in the subarctic North Pacific, this signal was initially associated with low oxygen waters of the North Pacific OMZ and interpreted to be the result of CdS precipitation within sinking particles (Janssen et al., 2014). However, our data show that the Cd* signal is not limited to low oxygen waters but instead spans the entire eastern North Pacific, coinciding with the PO$_4$ maximum (Figure 8). Indeed, isopycnal systematics (Figure 9) reveal that this Cd* signal is associated with the same density range as the PO$_4$ maximum, which characterizes PDW. Importantly, the deep Pacific Cd:PO$_4$ ratio (0.35 mmol mol^{-1}) that we use to calculate Cd* is set during water mass formation in the Southern Ocean (Sieber, Conway, de Souza, Obata, et al., 2019). Because Cd systematics in North Pacific deep waters (below 2,000 m) are predominantly controlled by internal mixing of preformed, southern-sourced water mass signatures, these waters show no meridional change throughout the Pacific Ocean (Section 4.2, Sieber, Conway, de Souza, Obata, et al., 2019). However, the core of PDW contains a significant amount of regenerated Cd and PO$_4$ (up to 30%), which reflects an integrated regeneration signal of the Pacific. Hence, we suggest that the deeper Cd* minimum is associated with PDW as a consequence of regeneration of Cd and PO$_4$ at a slightly lower ratio than 0.35 mmol mol^{-1} integrated across the Pacific, rather than relating to processes in low-oxygen waters. Overall, this is consistent with patterns of Cd:P export ratios (Black et al., 2019) and euphotic-zone particulate Cd:P ratios (Bourne et al., 2018) in Pacific oligotrophic waters, which are an order of magnitude lower than in HNLC regimes. LCDW is formed in the Southern Ocean, an HNLC region with high Cd uptake relative to PO$_4$ (Baars et al., 2014), and while regeneration dominantly occurs in the shallow subsurface (Sieber, Conway, de Souza, Hassler, et al., 2019), likely a small fraction of particulates with high Cd:P is ultimately transferred to the deep ocean here. Conversely, surface Cd is strongly depleted over large parts of the Pacific, especially the subtropical gyres, associated with the regeneration of particles with low Cd:P for these areas (Bourne et al., 2018; Quay et al., 2015). Therefore, an integrated regeneration signal of the Pacific that accumulates in PDW will likely carry a lower Cd:PO$_4$ ratio than that found in the deep Pacific Ocean.

Above the deeper Cd* minimum (shallower than 700 m), there is a clear north-south dichotomy in Cd* along the section (Figures 3 and 8), split where the North Equatorial Current crosses GP15 (~20°N) due to the presence of different intermediate water masses. In the north (stations 10–19) outside the North Pacific HNLC, Cd* remains at near zero values (200–700 m, −0.05 to 0 nmol kg^{-1}) due to the presence of NPIW (Figure 9, Section 4.2). A subsurface Cd* minimum (top 200 m), above NPIW, could be driven by the regeneration of particles with low Cd:P within the oligotrophic gyre (Bourne et al., 2018).

In the south (stations 19–39), the Cd* signal intensifies above PDW due to the advected Cd* signal carried by eqAAIW (500–1,000 m, −0.1 nmol kg^{-1}, Figures 3, 8, and 9). However, the Cd* signal intensifies further above the core of eqAAIW (salinity minimum), reaching a minimum of −0.3 nmol kg^{-1} at depths of 250–500 m, indicating that an additional process is driving the signal at these depths (Figures 8 and 9). A similar Cd* signal in the equatorial Pacific has been linked to a particle maximum occurring at the same depths and attributed to a process removing Cd from the water column (de Souza et al., 2022). While the cause of this removal process remains under debate, it has been suggested to be related to biological activity such as elevated Cd uptake relative to PO$_4$ by heterotrophic organisms (de Souza et al., 2022; Ohnemus et al., 2019). Alternatively, the decoupling of Cd and PO$_4$ in the tropical Pacific might be driven by differential remineralization of Cd and P in sinking particles (Laubach et al., 2022; Roshan & DeVries, 2021; Twining et al., 2015). In our data set, we find a consistent implied Cd loss process; however, it remains unclear which, if any, of these mechanisms may be driving this. As such, we anticipate that further targeted studies that integrate investigations of the Cd content and isotopic composition of the dissolved and particulate fractions in these low-latitude regions will be required to disentangle and understand these complex near-surface processes.

5. Conclusions

Here, we have presented dissolved Cd and δ^{114}Cd data from the US GEOTRACES GP15 meridional section along 152°W from the Alaskan shelf to the equatorial Pacific. Our data set highlights the importance of Southern Ocean processes and ocean circulation control for the distribution of Cd and δ^{114}Cd, even in the North Pacific.
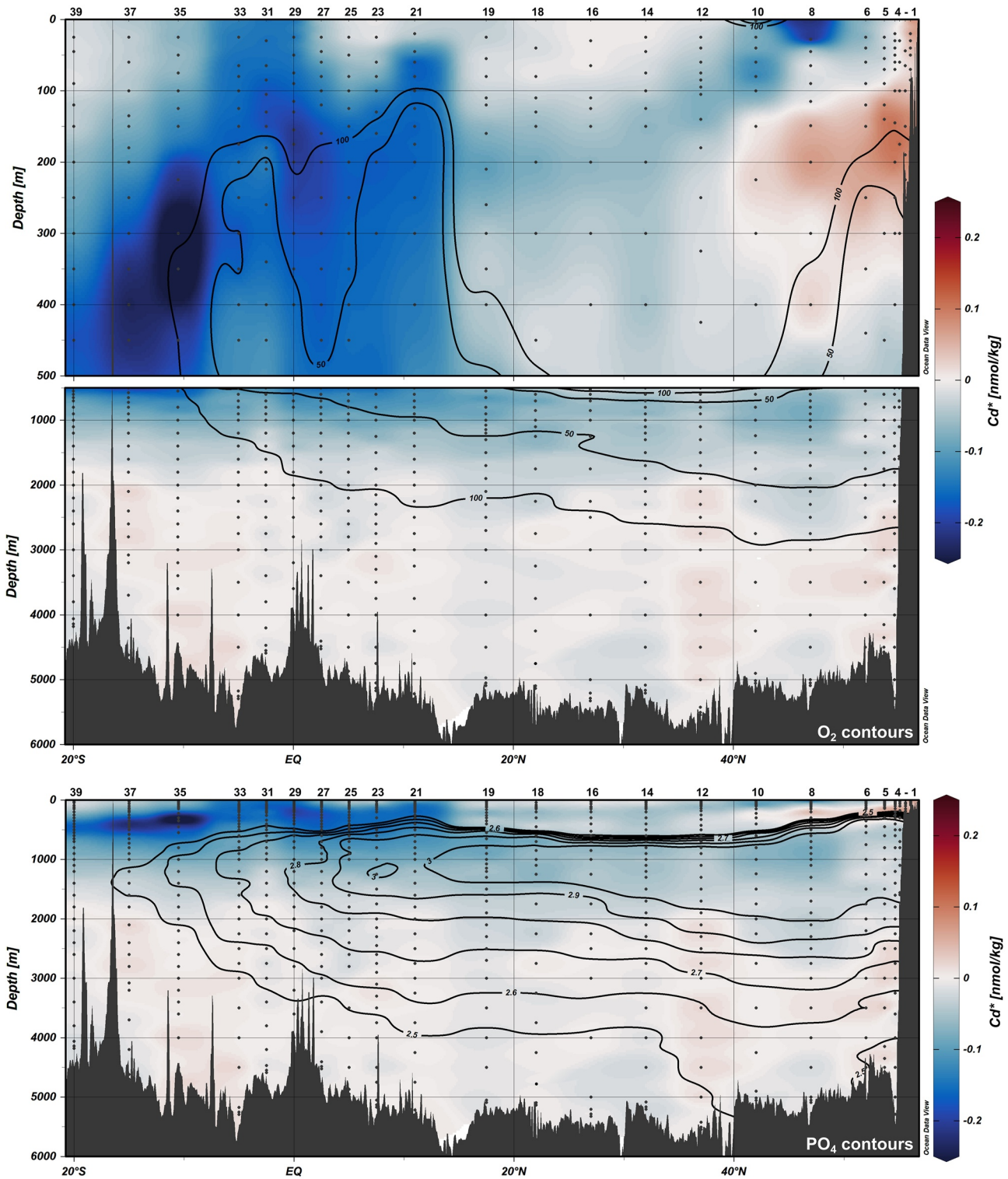
Figure 8. *GP15 Cd* distribution*. Cd* overlain with oxygen contours (top) and phosphate contours (bottom). Note the different depth scales for the upper (0–500) and deep ocean (500–6,000 m) in the top panel.
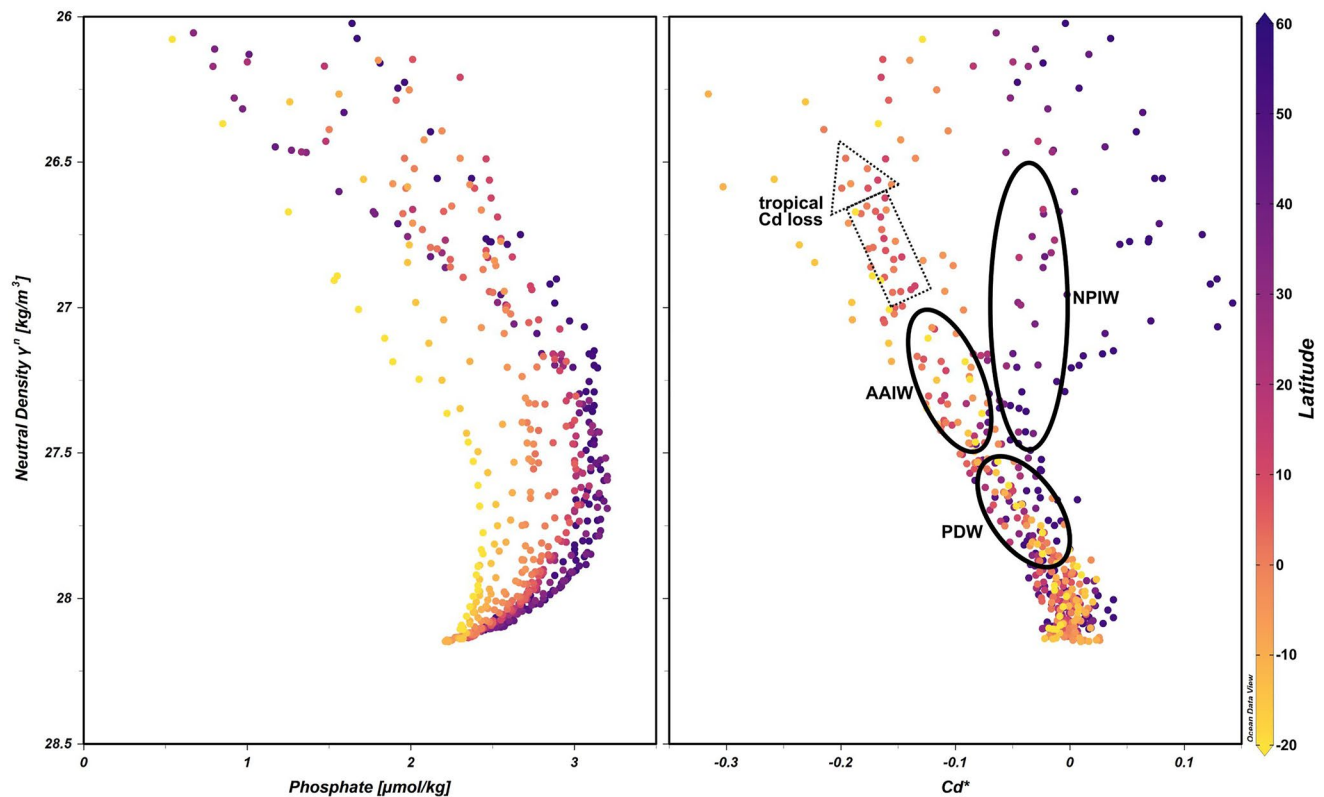
Figure 9. *Isopycnal Cd* systematics*. Phosphate and Cd* plotted against neutral density, color-coded for latitude. All data in the density range of the PO_4 maximum (27.5–27.8 kg m^{-3}) show a slightly negative Cd* signal. In the density range occupied by intermediate water masses (26.5–27.4 kg m^{-3}), the contrasting influence of Antarctic Intermediate Water (AAIW) and North Pacific Intermediate Water is reflected by divergence in Cd* between southern- and northern-sourced waters. A tropical Cd loss process (de Souza et al., 2022) drives Cd* to more negative values above AAIW in the equatorial Pacific.

Specifically, we show that AAIW has an important influence on $\delta^{114}Cd$ signatures in intermediate waters of the North Pacific subtropical gyre and is distinctly different from northern-sourced NPIW. Our examination of the surface Cd isotope systematics is consistent with previous observations, showing a stark disparity between Cd-rich HNLC waters and Cd-depleted waters of the subtropical and equatorial Pacific. However, we suggest that atmospheric inputs also play an important role in setting the surface $\delta^{114}Cd$ at the lowest Cd concentrations. Based upon our assessment of Cd* anomalies along GP15 in the context of a Southern Ocean determined Cd-PO_4 relationship, we propose that the negative Cd* signal at depth in the North Pacific is associated with the PO_4 maximum and is a consequence of an integrated regeneration signal of Cd and PO_4 at a slightly lower Cd:P ratio than the deep ocean ratio, rather than relating to processes in low-oxygen waters.

Globally, we now have a complete picture of the Cd distributions in the Atlantic and Pacific basins (Figure 10). Despite southern-sourced water masses supplying similar Cd signatures from the Southern Ocean into both basins (Abouchami et al., 2014; Sieber, Conway, de Souza, Hassler, et al., 2019), the distributions in the two basins are notably different. The disparity stems from the different deep water formation mechanisms in the north of each basin: active deep water formation in the North Atlantic entrains low Cd, high $\delta^{114}Cd$ upper ocean waters leading to lower Cd concentrations and elevated $\delta^{114}Cd$ throughout large parts of the deep Atlantic where NADW is the dominant water mass. The formation of PDW in the North Pacific however has no surface sources and consequently PDW is isotopically indistinguishable from southern-sourced deep waters as regeneration throughout the Pacific leads to an increase in Cd concentrations but does not change $\delta^{114}Cd$ (Janssen et al., 2017; Sieber, Conway, de Souza, Obata, et al., 2019). As a result, compared to the Southern Ocean (0.76 nmol kg^{-1}; +0.26‰: Sieber, Conway, de Souza, Hassler, et al., 2019), the deep Pacific is richer in Cd (0.76–1.05 nmol kg^{-1}) and isotopically homogeneous (+0.25‰) while the deep Atlantic carries lower Cd concentrations (0.27–0.78 nmol kg^{-1}) and elevated $\delta^{114}Cd$ (0.25‰–0.45‰, Xie et al., 2017). When considering a global deep ocean $\delta^{114}Cd$ average, NADW has little influence due to its low Cd concentration
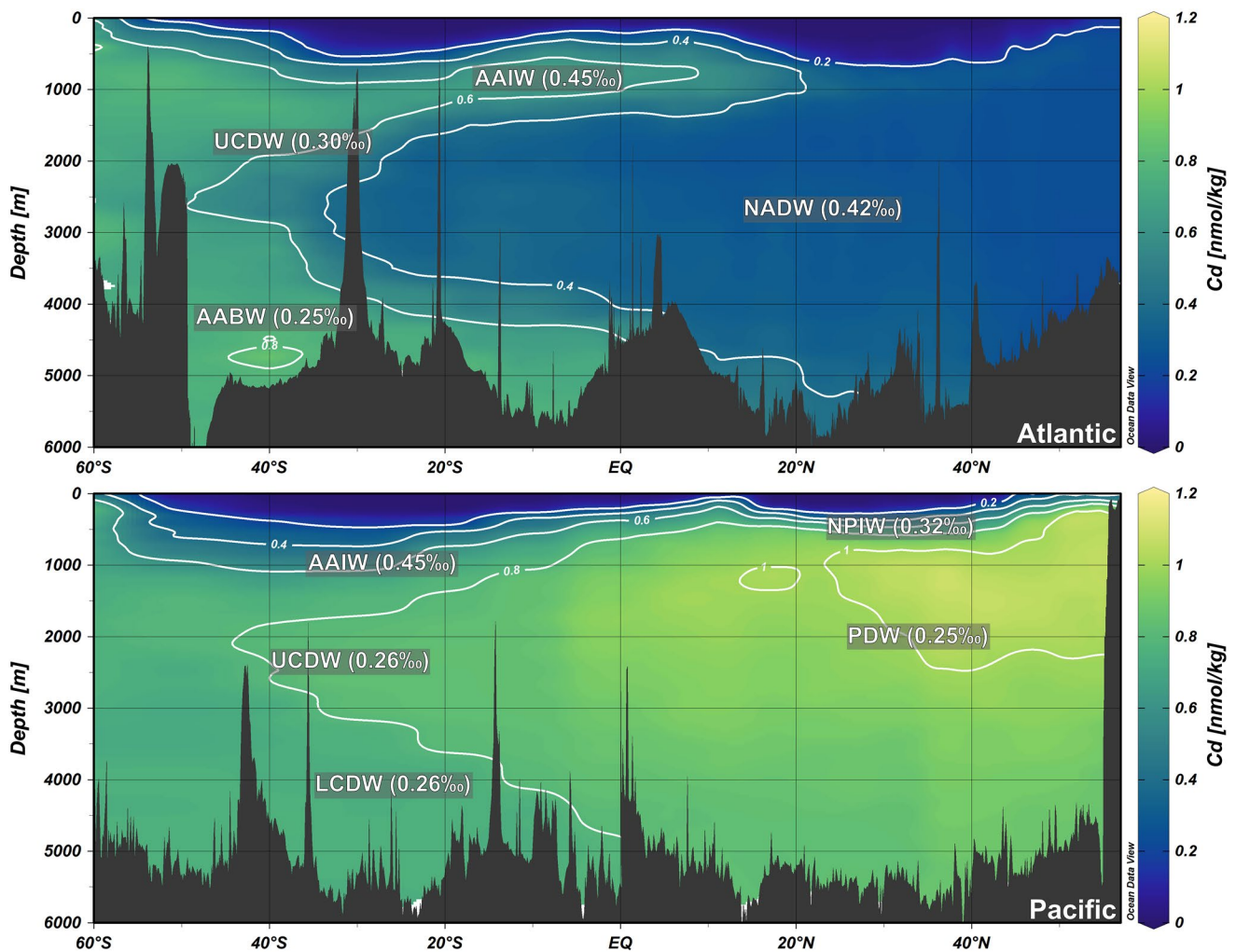
Figure 10. *Quasi-meridional Cd sections of the Atlantic and Pacific basin with the main water mass $\delta^{114}Cd$ signatures.* Cadmium concentration data are from this study and the GEOTRACES Intermediate Data Product 2021. Water mass signatures are based on this study, Xie et al. (2017), Yang et al. (2018), and Sieber, Conway, de Souza, Obata et al. (2019).

compared to other deep waters, despite its elevated $\delta^{114}Cd$. Even if we only take into account the volumes of NADW and Antarctic Bottom Water (AABW; Johnson, 2008) and use their endmember compositions (Figure 10) to estimate a global deep water $\delta^{114}Cd$ average, we obtain an average of +0.28‰, which is not resolvable from the average $\delta^{114}Cd$ of the deep Southern Ocean and Pacific (Sieber, Conway, de Souza, Obata, et al., 2019). Since this approach only considers two water masses it likely underestimates the impact of Cd-rich Pacific waters, and, hence, we suggest +0.25‰ ± 0.04‰ (mean of IDP2021 and this study, data >2,000 m, excluding the Atlantic Ocean, 1SD, $n = 538$) as an estimate of the average $\delta^{114}Cd$ of the modern deep ocean.

Data Availability Statement

The data set measured at USF is available on the BCO-DMO website (https://www.bco-dmo.org/dataset/883862 and https://www.bco-dmo.org/dataset/884673). Data sets measured at USC and TAMU will be available on the BCO-DMO website as well.

References

Abouchami, W., Galer, S. J. G., de Baar, H. J. W., Alderkamp, A. C., Middag, R., Laan, P., et al. (2011). Modulation of the Southern Ocean cadmium isotope signature by ocean circulation and primary productivity. *Earth and Planetary Science Letters*, *305*(1–2), 83–91. https://doi.org/10.1016/j.epsl.2011.02.044

Abouchami, W., Galer, S. J. G., De Baar, H. J. W., Middag, R., Vance, D., Zhao, Y., et al. (2014). Biogeochemical cycling of cadmium isotopes in the Southern Ocean along the zero meridian. *Geochimica et Cosmochimica Acta*, *127*, 348–367. https://doi.org/10.1016/j.gca.2013.10.022

Abouchami, W., Galer, S. J. G., Horner, T. J., Rehkämper, M., Wombacher, F., Xue, Z., et al. (2013). A common reference material for cadmium isotope studies - NIST SRM 3108. *Geostandards and Geoanalytical Research*, *37*(1), 5–17. https://doi.org/10.1111/j.1751-908X.2012.00175.x

Baars, O., Abouchami, W., Galer, S. J. G., Boye, M., & Croot, P. L. (2014). Dissolved cadmium in the Southern Ocean: Distribution, speciation, and relation to phosphate. *Limnology and Oceanography*, *59*(2), 385–399. https://doi.org/10.4319/lo.2014.59.2.0385

Bathen, K. H. (1972). On the seasonal changes in the depth of the mixed layer in the North Pacific Ocean. *Journal of Geophysical Research*, *77*(36), 7138–7150. https://doi.org/10.1029/JC077i036p07138

Bernhardt, H., & Wilhelms, A. (1967). The continuous determination of low level iron, soluble phosphate, and total phosphate with the AutoAnalyzer. In *Technicon symposia* (Vol. 1, pp. 385–389).

Black, E. E., Lam, P. J., Lee, J. M., & Buesseler, K. O. (2019). Insights from the ^{238}U-^{234}Th method into the coupling of biological export and the cycling of cadmium, cobalt, and manganese in the Southeast Pacific Ocean. *Global Biogeochemical Cycles*, *33*(1), 15–36. https://doi.org/10.1029/2018GB005985

Bourne, H. L., Bishop, J. K. B., Lam, P. J., & Ohnemus, D. C. (2018). Global spatial and temporal variation of Cd:P in euphotic zone particulates. *Global Biogeochemical Cycles*, *32*(7), 1123–1141. https://doi.org/10.1029/2017GB005842

Boyle, E. A., Sclater, F., & Edmond, J. M. (1976). On the marine geochemistry of cadmium. *Nature*, *263*(5572), 42–44. https://doi.org/10.1038/263042a0

Brand, L. E., Sunda, W. G., & Guillard, R. R. L. (1986). Reduction of marine phytoplankton reproduction rates by copper and cadmium. *Journal of Experimental Marine Biology and Ecology*, *96*(3), 225–250. https://doi.org/10.1016/0022-0981(86)90205-4

Bridgestock, L., Rehkämper, M., van de Flierdt, T., Murphy, K., Khondoker, R., Baker, A. R., et al. (2017). The Cd isotope composition of atmospheric aerosols from the Tropical Atlantic Ocean. *Geophysical Research Letters*, *44*(6), 2932–2940. https://doi.org/10.1002/2017GL072748

Bruland, K. W. (1980). Oceanographic distributions of cadmium, zinc, nickel, and copper in the North Pacific. *Earth and Planetary Science Letters*, *47*(2), 176–198. https://doi.org/10.1016/0012-821X(80)90035-7

Bruland, K. W., Orians, K. J., & Cowen, J. P. (1994). Reactive trace-metals in the stratified central North Pacific. *Geochimica et Cosmochimica Acta*, *58*(15), 3171–3182. https://doi.org/10.1016/0016-7037(94)90044-2

Buck, C. S., Landing, W. M., & Resing, J. (2013). Pacific Ocean aerosols: Deposition and solubility of iron, aluminum, and other trace elements. *Marine Chemistry*, *157*, 117–130. https://doi.org/10.1016/j.marchem.2013.09.005

Cloquet, C., Carignan, J., Libourel, G., Sterckeman, T., & Perdrix, E. (2006). Tracing source pollution in soils using cadmium and lead isotopes. *Environmental Science & Technology*, *40*(8), 2525–2530. https://doi.org/10.1021/es052232+

Conway, T. M., & John, S. G. (2015a). Biogeochemical cycling of cadmium isotopes along a high-resolution section through the North Atlantic Ocean. *Geochimica et Cosmochimica Acta*, *148*, 269–283. https://doi.org/10.1016/j.gca.2014.09.032

Conway, T. M., & John, S. G. (2015b). The cycling of iron, zinc and cadmium in the North East Pacific Ocean - Insights from stable isotopes. *Geochimica et Cosmochimica Acta*, *164*, 262–283. https://doi.org/10.1016/j.gca.2015.05.023

Cullen, J. T. (2006). On the nonlinear relationship between dissolved cadmium and phosphate in the modern global ocean: Could chronic iron limitation of phytoplankton growth cause the kink? *Limnology and Oceanography*, *51*(3), 1369–1380. https://doi.org/10.4319/lo.2006.51.3.1369

Cullen, J. T., Chase, Z., Coale, K. H., Fitzwater, S. E., & Sherrell, R. M. (2003). Effect of iron limitation on the cadmium to phosphorus ratio of natural phytoplankton assemblages from the Southern Ocean. *Limnology and Oceanography*, *48*(3), 1079–1087. https://doi.org/10.4319/lo.2003.48.3.1079

Cutter, G. A., & Bruland, K. W. (2012). Rapid and noncontaminating sampling system for trace elements in global ocean surveys. *Limnology and Oceanography: Methods*, *10*(6), 425–436. https://doi.org/10.4319/lom.2012.10.425

de Baar, H. J. W., Saager, P. M., Nolting, R. F., & van der Meer, J. (1994). Cadmium versus phosphate in the world ocean. *Marine Chemistry*, *46*(3), 261–281. https://doi.org/10.1016/0304-4203(94)90082-5

de Souza, G. F., Vance, D., Sieber, M., Conway, T. M., & Little, S. H. (2022). Re-assessing the influence of particle-hosted sulphide precipitation on the marine cadmium cycle. *Geochimica et Cosmochimica Acta*, *322*, 274–296. https://doi.org/10.1016/j.gca.2022.02.009

Favorite, F., & Ingraham, W. J. (1977). On flow in Northwestern Gulf of Alaska, may 1972. *Journal of the Oceanographical Society of Japan*, *33*(2), 67–81. https://doi.org/10.1007/BF02110012

Fuhr, M., Laukert, G., Yu, Y., Nürnberg, D., & Frank, M. (2021). Tracing water mass mixing from the equatorial to the North Pacific Ocean with dissolved Neodymium isotopes and concentrations. *Frontiers in Marine Science*, *7*, 1–18. https://doi.org/10.3389/fmars.2020.603761

Gault-Ringold, M., Adu, T., Stirling, C. H., Frew, R. D., & Hunter, K. A. (2012). Anomalous biogeochemical behavior of cadmium in subantarctic surface waters: Mechanistic constraints from cadmium isotopes. *Earth and Planetary Science Letters*, *341344*, 94–103. https://doi.org/10.1016/j.epsl.2012.06.005

George, E., Stirling, C. H., Gault-Ringold, M., Ellwood, M. J., & Middag, R. (2019). Marine biogeochemical cycling of cadmium and cadmium isotopes in the extreme nutrient-depleted subtropical gyre of the South West Pacific Ocean. *Earth and Planetary Science Letters*, *514*, 84–95. https://doi.org/10.1016/J.EPSL.2019.02.031

Guinoiseau, D., Galer, S. J. G. G., Abouchami, W., Frank, M., Achterberg, E. P., & Haug, G. H. (2019). Importance of cadmium sulfides for biogeochemical cycling of Cd and its isotopes in oxygen deficient zones—A case study of the Angola Basin. *Global Biogeochemical Cycles*, *33*(12), 1746–1763. https://doi.org/10.1029/2019GB006323

Horner, T. J., Lee, R. B. Y., Henderson, G. M., & Rickaby, R. E. M. (2013). Nonspecific uptake and homeostasis drive the oceanic cadmium cycle. *Proceedings of the National Academy of Sciences of the United States of America*, *110*(7), 2500–2505. https://doi.org/10.1073/pnas.1213857110

Janssen, D. J., Abouchami, W., Galer, S. J. G., & Cullen, J. T. (2017). Fine-scale spatial and interannual cadmium isotope variability in the subarctic northeast Pacific. *Earth and Planetary Science Letters*, *472*, 241–252. https://doi.org/10.1016/j.epsl.2017.04.048

Janssen, D. J., Conway, T. M., John, S. G., Christian, J. R., Kramer, D. I., Pedersen, T. F., & Cullen, J. T. (2014). Undocumented water column sink for cadmium in open ocean oxygen-deficient zones. *Proceedings of the National Academy of Sciences of the United States of America*, *111*(19), 6888–6893. https://doi.org/10.1073/pnas.1402388111

Jensen, L. T., Wyatt, N. J., Landing, W. M., & Fitzsimmons, J. N. (2020). Assessment of the stability, sorption, and exchangeability of marine dissolved and colloidal metals. *Marine Chemistry*, *220*, 103754. https://doi.org/10.1016/j.marchem.2020.103754

John, S. G., & Conway, T. M. (2014). A role for scavenging in the marine biogeochemical cycling of zinc and zinc isotopes. *Earth and Planetary Science Letters*, *394*, 159–167. https://doi.org/10.1016/j.epsl.2014.02.053

John, S. G., Helgoe, J., & Townsend, E. (2018). Biogeochemical cycling of Zn and Cd and their stable isotopes in the Eastern Tropical South Pacific. *Marine Chemistry*, *201*, 256–262. https://doi.org/10.1016/J.MARCHEM.2017.06.001

Johnson, G. C. (2008). Quantifying Antarctic bottom water and North Atlantic deep water volumes. *Journal of Geophysical Research*, *113*(C5), 1–13. https://doi.org/10.1029/2007JC004477

Kawabe, M., & Fujio, S. (2010). Pacific Ocean circulation based on observation. *Journal of Oceanography*, *66*(3), 389–403. https://doi.org/10.1007/s10872-010-0034-8

Lacan, F., Francois, R., Ji, Y., & Sherrell, R. (2006). Cadmium isotopic composition in the ocean. *Geochimica et Cosmochimica Acta*, *70*(20), 5104–5118. https://doi.org/10.1016/j.gca.2006.07.036

Lagerström, M. E., Field, M. P., Séguret, M., Fischer, L., Hann, S., & Sherrell, R. M. (2013). Automated on-line flow-injection ICP-MS determination of trace metals (Mn, Fe, Co, Ni, Cu and Zn) in open ocean seawater: Application to the GEOTRACES program. *Marine Chemistry*, *155*, 71–80. https://doi.org/10.1016/J.MARCHEM.2013.06.001

Lambelet, M., Rehkämper, M., van de Flierdt, T., Xue, Z., Kreissig, K., Coles, B., et al. (2013). Isotopic analysis of Cd in the mixing zone of Siberian rivers with the Arctic Ocean-New constraints on marine Cd cycling and the isotope composition of riverine Cd. *Earth and Planetary Science Letters*, *361*, 64–73. https://doi.org/10.1016/j.epsl.2012.11.034

Laubach, A., Lee, J.-M., & Lam, P. (2022). Particulate Cd:P on three U.S. GEOTRACES cruises. In *Abstract presented at 2022 Ocean Sciences Meeting*, 28 Feb. - 4 Mar.

Marsay, C. M., Kadko, D., Landing, W. M., & Buck, C. S. (2022). Bulk aerosol trace element concentrations and deposition fluxes during the U.S. GEOTRACES GP15 Pacific meridional transect. *Global Biogeochemical Cycles*, *36*(2), 1–20. https://doi.org/10.1029/2021gb007122

Middag, R., van Heuven, S. M. A. C., Bruland, K. W., & de Baar, H. J. W. (2018). The relationship between cadmium and phosphate in the Atlantic Ocean unravelled. *Earth and Planetary Science Letters*, *492*, 79–88. https://doi.org/10.1016/J.EPSL.2018.03.046

Ohnemus, D. C., Torrie, R., & Twining, B. S. (2019). Exposing the distributions and elemental associations of scavenged particulate phases in the ocean using basin-scale multi-element data sets. *Global Biogeochemical Cycles*, *33*(6), 725–748. https://doi.org/10.1029/2018GB006145

Price, N. M., & Morel, F. M. M. (1990). Cadmium and cobalt substitution for zinc in a marine diatom. *Nature*, *344*(6267), 658–660. https://doi.org/10.1038/344658a0

Quay, P., Cullen, J. T., Landing, W., & Morton, P. (2015). Processes controlling the distributions of Cd and PO_4 in the ocean. *Global Biogeochemical Cycles*, *29*(6), 830–841. https://doi.org/10.1002/2013GB004593.Received

Rehkämper, M., Wombacher, F., Horner, T. J., & Xue, Z. (2012). Natural and anthropogenic Cd isotope variations. In M. Baskaran (Ed.), *Handbook of environmental Isotope geochemistry* (pp. 125–154). Springer. https://doi.org/10.1007/978-3-642-10637-8

Ripperger, S., & Rehkämper, M. (2007). Precise determination of cadmium isotope fractionation in seawater by double spike MC-ICPMS. *Geochimica et Cosmochimica Acta*, *71*(3), 631–642. https://doi.org/10.1016/j.gca.2006.10.005

Roden, G. I. (1975). On North Pacific temperature, salinity, sound velocity and density fronts and their relation to the wind and energy flux fields. *Journal of Physical Oceanography*, *5*(4), 557–571. https://doi.org/10.1175/1520-0485(1975)005<0557:onptss>2.0.co;2

Roshan, S., & DeVries, T. (2021). Global contrasts between oceanic cycling of cadmium and phosphate. *Global Biogeochemical Cycles*, *35*(6), 1–18. https://doi.org/10.1029/2021GB006952

Roshan, S., & Wu, J. (2015). Cadmium regeneration within the North Atlantic. *Global Biogeochemical Cycles*, *29*(12), 2082–2094. https://doi.org/10.1002/2015GB005215

Rudnick, R. L., & Gao, S. (2013). Composition of the continental crust. In *Treatise on geochemistry* (2nd ed.). Elsevier Ltd. https://doi.org/10.1016/B978-0-08-095975-7.00301-6

Sallée, J.-B., Speer, K., Rintoul, S., & Wijffels, S. (2010). Southern Ocean thermocline ventilation. *Journal of Physical Oceanography*, *40*(3), 509–529. https://doi.org/10.1175/2009JPO4291.1

Sieber, M., Conway, T. M., de Souza, G. F., Hassler, C. S., Ellwood, M. J., & Vance, D. (2019). High-resolution Cd isotope systematics in multiple zones of the Southern Ocean from the Antarctic circumnavigation expedition. *Earth and Planetary Science Letters*, *527*, 115799. https://doi.org/10.1016/J.EPSL.2019.115799

Sieber, M., Conway, T. M., de Souza, G. F. F., Obata, H., Takano, S., Sohrin, Y., & Vance, D. (2019). Physical and biogeochemical controls on the distribution of dissolved cadmium and its isotopes in the Southwest Pacific Ocean. *Chemical Geology*, *511*, 494–509. https://doi.org/10.1016/j.chemgeo.2018.07.021

Sunda, W. G., & Huntsman, S. A. (2000). Effect of Zn, Mn, and Fe on Cd accumulation in phytoplankton: Implications for oceanic Cd cycling. *Limnology and Oceanography*, *45*(7), 1501–1516. https://doi.org/10.4319/lo.2000.45.7.1501

Talley, L. D., Pickard, G. L., Emery, W. J., & Swift, J. H. (2011). *Descriptive physical oceanography: An introduction*. Academic Press.

Twining, B. S., Rauschenberg, S., Morton, P. L., & Vogt, S. (2015). Metal contents of phytoplankton and labile particulate material in the North Atlantic Ocean. *Progress in Oceanography*, *137*, 261–283. https://doi.org/10.1016/j.pocean.2015.07.001

Vance, D., de Souza, G. F., Zhao, Y., Cullen, J. T., & Lohan, M. C. (2019). The relationship between zinc, its isotopes, and the major nutrients in the North-East Pacific. *Earth and Planetary Science Letters*, *525*, 115748. https://doi.org/10.1016/J.EPSL.2019.115748

Wu, J., & Roshan, S. (2015). Cadmium in the North Atlantic: Implication for global cadmium-phosphorus relationship. *Deep Sea Research Part II: Topical Studies in Oceanography*, *116*, 226–239. https://doi.org/10.1016/j.dsr2.2014.11.007

Xie, R. C., Galer, S. J. G., Abouchami, W., & Frank, M. (2018). Limited impact of eolian and riverine sources on the biogeochemical cycling of Cd in the tropical Atlantic. *Chemical Geology*, *511*, 371–379. https://doi.org/10.1016/J.CHEMGEO.2018.10.018

Xie, R. C., Galer, S. J. G., Abouchami, W., Rijkenberg, M. J. A., de Baar, H. J. W., De Jong, J., & Andreae, M. O. (2017). Non-Rayleigh control of upper-ocean Cd isotope fractionation in the Western South Atlantic. *Earth and Planetary Science Letters*, *471*, 94–103. https://doi.org/10.1016/j.epsl.2017.04.024

Xue, Z., Rehkämper, M., Schönbächler, M., Statham, P. J., & Coles, B. J. (2012). A new methodology for precise cadmium isotope analyses of seawater. *Analytical and Bioanalytical Chemistry*, *402*(2), 883–893. https://doi.org/10.1007/s00216-011-5487-0

Yang, S.-C., Zhang, J., Sohrin, Y., & Ho, T.-Y. (2018). Cadmium cycling in the water column of the Kuroshio-Oyashio Extension region: Insights from dissolved and particulate isotopic composition. *Geochimica et Cosmochimica Acta*, *233*, 66–80. https://doi.org/10.1016/J.GCA.2018.05.001

You, Y. (2003). The pathway and circulation of North Pacific intermediate water. *Geophysical Research Letters*, *30*, 24–27. https://doi.org/10.1029/2003GL018561

Zhong, Q., Zhou, Y., Tsang, D. C. W., Liu, J., Yang, X., Yin, M., et al. (2020). Cadmium isotopes as tracers in environmental studies: A review. *Science of the Total Environment*, *736*, 139585. https://doi.org/10.1016/j.scitotenv.2020.139585